Dendrimer-Based Multivalent Vancomycin Nanoplatform for Targeting the Drug-Resistant Bacterial Surface

Seok Ki Choi,[†,‡,*] Andrzej Myc,[†,‡,∥,*] Justin Ezekiel Silpe,[‡,§] Madhuresh Sumit,[‡,⊥] Pamela Tinmoi Wong,[†,‡] Kelly McCarthy,[‡] Ankur M. Desai,[†,‡] Thommey P Thomas,[†,‡] Alina Kotlyar,[†,‡] Mark M. Banaszak Holl,[‡,§,⊥,¶] Bradford G. Orr,[‡,#] and James R. Baker, Jr.[†,‡]

[†]Department of Internal Medicine, [‡]Michigan Nanotechnology Institute for Medicine and Biological Sciences, [§]Department of Macromolecular Science and Engineering, [⊥]Program in Biomedical Sciences, [¶]Department of Chemistry, and [#]Department of Physics, University of Michigan, Ann Arbor, Michigan 48109, United States, [∥]Department of Immunology of Infectious Diseases, Ludwik Hirszfeld Institute of Immunology and Experimental Therapy, Polish Academy of Sciences, Wroclaw, Poland

ABSTRACT Vancomycin represents the preferred ligand for bacteria-targeting nanosystems. However, it is inefficient for emerging vancomycin-resistant species because of its poor affinity to the reprogrammed cell wall structure. This study demonstrates the use of a multivalent strategy as an effective way for overcoming such an affinity limitation in bacteria targeting. We designed a series of fifth generation (G5) poly(amidoamine) (PAMAM) dendrimers tethered with vancomycin at the C-terminus at different valencies. We performed surface plasmon resonance (SPR) studies to determine their binding avidity to two cell wall models, each made with either a vancomycin-susceptible D-Ala-D-Ala or vancomycin-resistant D-Ala-D-Lac cell wall precursor. These conjugates showed remarkable enhancement in avidity in the cell wall models tested, including the vancomycin-resistant model, which had an increase in avidity of four to five orders of magnitude greater than free vancomycin. The tight adsorption of the conjugate to the model surface corresponded with its ability to bind vancomycin-susceptible *Staphylococcus aureus* bacterial cells *in vitro* as imaged by confocal fluorescent microscopy. This vancomycin platform was then used to fabricate the surface of iron oxide nanoparticles by coating them with the dendrimer conjugates, and the resulting dendrimer-covered magnetic nanoparticles were demonstrated to rapidly sequester bacterial cells. In summary, this article investigates the biophysical basis of the tight, multivalent association of dendrimer-based vancomycin conjugates to the bacterial cell wall, and proposes a potential new use of this nanoplatform in targeting Gram-positive bacteria.

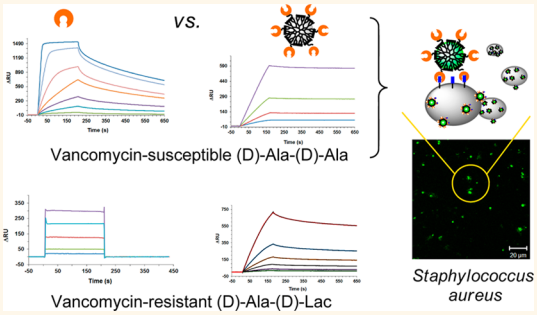

KEYWORDS: vancomycin · poly(amidoamine) dendrimer · surface plasmon resonance spectroscopy · bacterial cell wall · iron oxide nanoparticle

Gram-positive bacterial infections[1,2] cause numerous serious medical conditions including sepsis, bacteremia, pneumonia, and endocarditis.[3−6] Such infections can be life-threatening, especially when associated with drug-resistant bacteria.[3,7] Despite the fact that there are growing concerns about serious infectious diseases, current technology is not able to fully and accurately detect, enumerate, or treat those causative bacterial cells inhabiting the blood and other vital organs.[8] This report describes the biophysical evaluation and practical exploration of vancomycin-presenting, poly(amidoamine) (PAMAM) dendrimers as a new platform that enables detection and isolation of bacterial pathogens.

Recently, rapid advances have been made in cell-targeted delivery systems that cover a wide range of therapeutic areas from cancers and inflammatory diseases to infections.[9−13] Each delivery platform is typically composed of a nanometer-sized particle (NP) or scaffold conjugated with high affinity small molecule ligands or antibodies to bind to specific surface biomarkers.[11,14] This targeting strategy allows cell-specific delivery of payloads such as small molecule chemotherapeutics, therapeutic genes, and imaging molecules also carried by the nanoparticles.[10,11,15]

As a micrometer-sized organism, the bacterium expresses a high density of various surface molecules on its cell wall that serve as rich opportunities for selective recognition

* Address correspondence to skchoi@umich.edu, myca@umich.edu.

Received for review August 25, 2012 and accepted December 6, 2012.

Published online December 24, 2012
10.1021/nn3038995

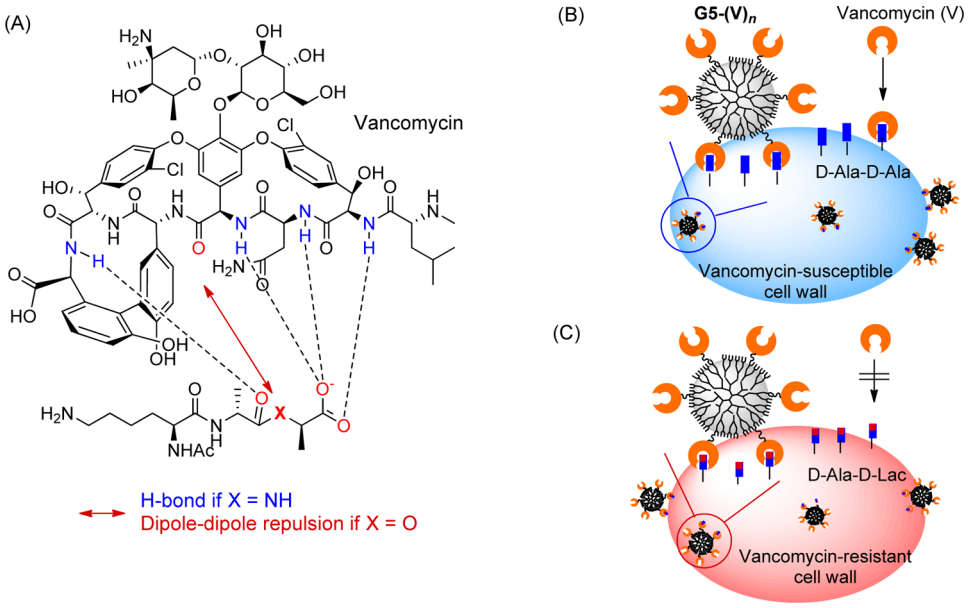

Figure 1. (A) Molecular mechanism for the recognition of the bacterial cell wall by the antibiotic vancomycin. The vancomycin molecule binds to the N^{α}-Ac-Lys-(D)-Ala-(D)-Ala terminus (X = NH; $K_D \approx 10^{-6}$ M) through five hydrogen bond (H bond) interactions, but such interactions are disrupted by the lactate (Lac; X = O; $K_D \approx 10^{-3}$ M)) exploited in the vancomycin-resistant bacterial cell wall which utilizes instead the N^{α}-Ac-Lys-(D)-Ala-(D)-Lac. (B, C) A schematic illustrating the proposed multivalent strategy for tight binding to Gram-positive bacterial cells by using a fifth generation (G5) PAMAM dendrimer conjugated with multiple copies of vancomycin molecules. Such multivalent vancomycin conjugates confer high avidity binding to the bacterial surface and enable them to target both vancomycin-susceptible and vancomycin-resistant bacterial cells. The size of the cell and the dendrimer particle are not drawn to scale.

of the cell. In fact, the modes of action associated with standard antimicrobial agents are attributable to binding and destabilization of the cell wall structure as seen with vancomycin,[16] beta-lactams,[17] and polymyxins.[18] Of these agents, vancomycin has been investigated as a molecular probe for targeting Gram-positive bacteria because of its strong affinity to a cell wall precursor terminated with a (D)-Ala-(D)-Ala peptide residue (Ala = alanine; Figure 1; $K_D \approx 10^{-6}$ M).[9,19−21] A few earlier studies reported on the practical applications of multivalent vancomycin molecules[22−26] as well as vancomycin-conjugated NPs which are made on the scaffold of poly(acrylamide) polymers,[20,21] and by direct attachment to the surface of inorganic NPs of gold[27] and iron oxide.[9,28] These studies demonstrated the effectiveness of such vancomycin conjugates in inducing bacteria-targeted opsonization activity,[20,21] enhancing antimicrobial activity,[27] and enabling the concentration of bacterial cells.[9,28]

Despite such strong potential demonstrated for cell wall-associated applications, vancomycin is not active against vancomycin-resistant *enterococci* (VRE) because it has weak affinity to the (D)-Ala-(D)-Lac residue (Lac = lactate; $K_D \approx 10^{-3}$ M) present on the bacterial surface of this species, resulting in vancomycin resistance.[16,29] In the present study, we apply a multivalent ligand design[30−33] for vancomycin and test the hypothetical notion that the suboptimal affinity of vancomycin can be enhanced by the use of a multivalent dendrimer. Defined as a molecular construct that presents multiple copies of an identical ligand tethered to a scaffold,[32−35] the multivalent molecule binds simultaneously to multiple receptors on the biological surface and, as a consequence, displays collectively much tighter binding avidity than the affinity displayed by each monovalent ligand attached. This multivalent concept has made a significant contribution to the design of potent inhibitors and effectors in the control of receptor−ligand interactions, pathogen-cell adhesion, and cellular uptake of NPs.[32,33,35]

Here, we focus on a fifth generation (G5) PAMAM dendrimer as the scaffold for the multivalent vancomycin design. As a synthetic polymer NP (diameter ≈ 5.4 nm),[36,37] the G5 dendrimer has been extensively investigated for use in applications in targeted drug delivery.[10,13,15,31,38−40] Its structure is characterized by a globular shape with a large number of peripheral branches amenable for chemical modifications and drug conjugation.[10,37,41,42] In addition, its terminal branches are organized in a predefined orientation, and constitute a platform preferred for multivalent presentation of vancomycin (Figure 1). This class of dendrimer conjugates is completely water-soluble and structurally tunable for controlling the valency, allowing for the systematic investigation of valency-avidity correlation by surface plasmon resonance (SPR) spectroscopy.

In the present article, we report the design and characterization of vancomycin-conjugated G5 PAMAM

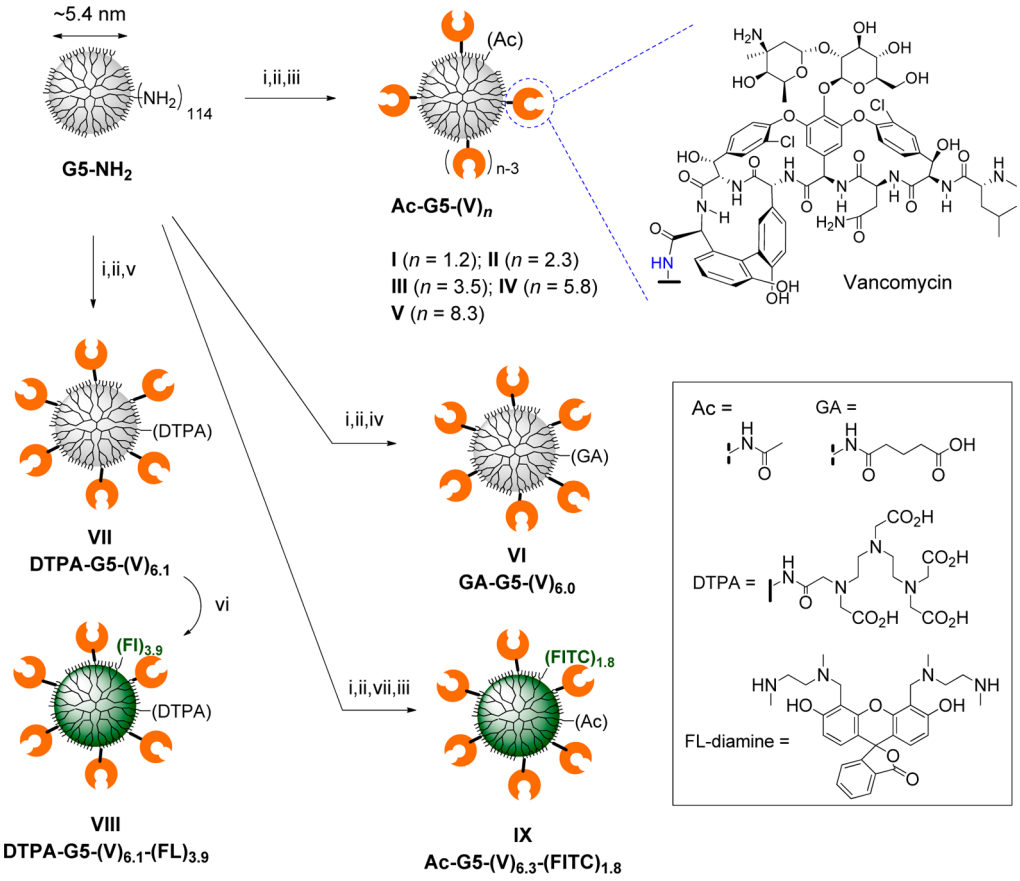

Scheme 1. Synthesis of vancomycin-conjugated G5 PAMAM dendrimers I–IX, each linked with the vancomycin molecule at the C-terminus through an amide bond in which V refers to vancomycin. Reagents and conditions: (i) vancomycin hydrochloride, *N*,*N*-diisopropyl-*N*-ethylamine (DIPEA), *N*-hydroxybenzotriazole (HOBt), benzotriazol-1-yl-oxytripyrrolidinophosphonium hexafluorophosphate (PyBOP), DMSO, DMF, 40 min, RT; (ii) G5-$(NH_2)_{114}$, MeOH, 5 h, RT ([Vancomycin]/[G5] = 1.2, 2.5, 5, 8, 10); (iii) Ac_2O, DIPEA, 1 h, RT; (iv) glutaric anhydride, DIPEA, 4 h, RT; (v) diethylenetriaminepentaacetic acid (DTPA) dianhydride, DIPEA, 12 h, RT; (vi) FL-diamine, DIPEA, HOBt, PyBOP, DMF, 24 h, RT; (vii) fluorescein 5(6)-isothiocyanate (FITC).

dendrimers G5-$(V)_n$ where V refers to vancomycin and each conjugate is varied as a function of vancomycin valency (*n*). We investigate the biophysical basis of the multivalency–avidity relationship, studied with two distinct bacterial cell wall models by SPR spectroscopy. We demonstrate the practicality of this dendrimer nanotechnology for fluorescent detection and magnetic sequestration of Gram-positive bacterial cells *in vitro*.

RESULTS AND DISCUSSION

Design and Synthesis of Vancomycin-Conjugated PAMAM Dendrimers. The current dendrimer platform used for vancomycin conjugation is based on G5 PAMAM dendrimer (G5-NH_2).[37,43] This dendrimer generation provides a sufficient number of peripheral branches (theoretically 128),[44,45] each terminated with a primary amine amenable to covalent conjugation with a variety of targeting ligands and drug molecules.[38,46–48] Our approach in the design of vancomycin-presenting G5 dendrimer conjugates involves two molecular parameters pertinent to vancomycin (Scheme 1): (i) the C-terminus as the position for vancomycin attachment and (ii) variation of the multivalency. First, we prepared a series of Ac-G5-$(V)_n$ conjugates **I**–**V**, each of which contains multiple vancomycin molecules at a variable mean valency. This series was prepared by preactivation of vancomycin by benzotriazol-1-yl-oxytripyrrolidinophosphonium hexafluorophosphate (PyBOP) and *N*-hydroxybenzotriazole (HOBt) as described elsewhere,[30,49] and subsequently by conjugation to the G5 PAMAM dendrimer through an amide bond. After this coupling step, each of the unreacted primary amines on the dendrimer was converted to an *N*-acetyl amide after treatment with acetic anhydride, making the dendrimer surface neutral. By varying the molar ratio of the two reactants ([Vancomycin]/[G5-NH_2] = 1.2, 2.5, 5, 8, and 10), it was possible to control the vancomycin valency that led to five different mean valencies of Ac-G5-$(V)_n$ (*n* = 1.2, 2.3, 3.5, 5.8, and 8.3).

This synthetic method was slightly modified to alter the physicochemical property of the dendrimer surface and also to introduce other functional moieties on the surface for enabling multifunctional applications. Thus two negatively charged conjugates, **VI** GA-G5-$(V)_6$ and **VII** DTPA-G5-$(V)_{6.1}$, were prepared by replacing the

acetic anhydride used in the second step with glutaric anhydride or diethylenetriaminepentaacetic acid (DTPA), respectively. The DTPA group present in the latter conjugate allows metal chelation with Gd(III) ions[50] and provides magnetic resonance imaging (MRI) capability potentially applicable for *in vivo* detection and imaging of bacterial cells. Those carboxylic acids localized on the dendrimer surface of **VI** and **VII** could be used for further derivatization, as illustrated by the synthesis of conjugate **VIII**, DTPA-G5-$(V)_{6.1}$-$(Fl)_{3.9}$, which carries fluorescein imaging molecules (FL-diamine; excitation/emission wavelength = 494 nm/518 nm).[51] In another approach for conjugation with fluorescent dye molecules, the primary amines of the dendrimer reacted directly with fluorescein isothiocyanate (FITC) prior to the last exhaustive N-acetylation step that led to the conjugate **IX** Ac-G5-$(V)_{6.3}$-$(FITC)_{1.8}$.

Purification of each vancomycin-conjugated dendrimer was performed by dialysis using a membrane tubing (molecular weight cut off or MWCO = 10 kDa) until its purity was greater than 95% as determined by the HPLC method (Supporting Information, Figure S2). Each of these conjugates **I**–**IX** was fully characterized by standard analytical methods including matrix assisted laser desorption ionization time-of-flight (MALDI TOF) spectrometry, ^{1}H NMR spectroscopy, and UV–vis spectrometry, as illustrated by the vancomycin-associated protons in the ^{1}H NMR spectral data and by the strong UV absorption features that are consistent with vancomycin (λ_{max} = 282 nm; ε = 6716 M^{-1} cm^{-1}) (see Supporting Information). In addition to MALDI measurement, selected members of the vancomycin conjugates were also characterized by using gel permeation chromatography (GPC) in order to measure their MWs and to determine the size distribution (Table 1). As summarized, the two sets of MWs, each determined independently by either MALDI or GPC, show similar MWs with generally narrow standard deviations lying within ±3 to 14% of their mean value. The vancomycin valency determined for each dendrimer conjugate is reported on a mean basis. These values were calculated by the analysis of the UV–vis absorptivity at 282 nm, but their determination by the alternative NMR method[44,45,52] was not attempted because of line broadening, signal overlaps, and unpredictable shifts of the vancomycin proton signals. The percent efficiency for vancomycin conjugation ($([V]_{attached} \div [V]_{added}) \times 100$; V = vancomycin) was in the range of 70–100%. A greater conjugation efficiency (>92%) was observed with the lower-valent conjugates **I** and **II**. Such trends might be attributable in part to the influence of steric congestion on the reactions occurring on the dendrimer surface,[53] which should be more serious as more molecules are conjugated.[36,37]

Distribution of Vancomycin Valency. Currently only a few specialized methods are demonstrated for the engineering and functionalization of NPs with a precise number of ligands or drugs, such as those for PAMAM dendrimer,[44,45,52] polymer,[54] or gold.[55,56] Otherwise all NP conjugation reactions, including the amide coupling reaction used for the current conjugate synthesis, occur with a stochastic mechanism that leads to a distribution of conjugate populations comprising variable range of ligand and drug valencies.[45,52] Therefore, a method for describing such dendrimer distributions differs from the way the mean valency (n) is determined and reported for each conjugate. Figure 2 shows the distribution of the dendrimers simulated for each of the conjugates **I**–**IV**, Ac-G5-$(V)_n$, according to a Poissonian simulation.[45,52] As an illustration, **I** Ac-G5-$(V)_n$ (n = 1.2) has approximately a valency of one vancomycin on an average basis but has a wider distribution including multivalent species (n = 0–7; median of valency = 4). Significantly, its populations of multivalent species ($n \geq 2$) add up to ~34% (inset),

TABLE 1. Selected Macromolecular Properties of PAMAM Dendrimers Conjugated with Vancomycin (V) Molecules

ID	dendrimer-$(V)_n$	MW (g/mol)[a]	MW_w[b] (PDI[c])	valency (n)[d]
I	Ac-G5-$(V)_{1.2}$	31100	37800 (1.067)	1
II	Ac-G5-$(V)_{2.3}$	32400	37600 (1.628)	2
III	Ac-G5-$(V)_{3.5}$	32300	30700 (1.043)	4
IV	Ac-G5-$(V)_{5.8}$	36300	37800 (1.027)	6
V	Ac-G5-$(V)_{8.3}$	37500	33200 (1.032)	8
VI	GA-G5-$(V)_{6.0}$	37100		6
VII	DTPA-G5-$(V)_{6.1}$		62500 (1.088)	6
VIII	DTPA-G5-$(V)_{6.1}$-$(Fl)_{3.9}$			6
IX	Ac-G5-$(V)_{6.3}$-$(FITC)_{1.8}$	36300		6

[a] Measured by matrix assisted laser desorption ionization (MALDI) mass spectrometry. [b] Weight-averaged molecular weight determined by gel permeation chromatography (GPC). [c] Polydispersity index (PDI) = $MW_w \div MW_n$. [d] Refers to number of vancomycin molecules attached to a dendrimer molecule determined by UV–vis spectrometry; each number calculated on a mean basis and rounded to the nearest whole number.

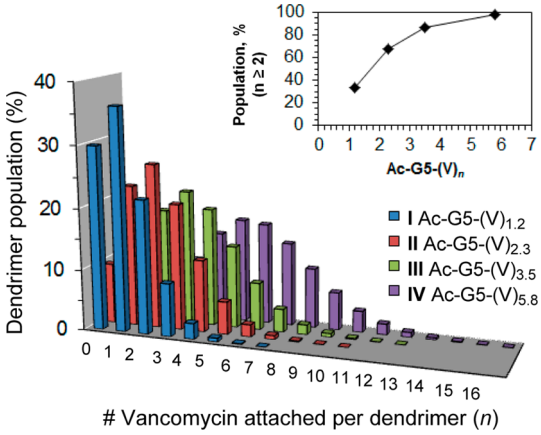

Figure 2. Poissonian distribution of Ac-G5-$(V)_n$ I–IV, each having the mean valency of vancomycin at 1, 2, 4, or 6, respectively. The sum of populations (%) of multivalent species Ac-G5-$(V)_n$ ($n \geq 2$) distributed in each conjugate I–IV is plotted in the inset.

suggesting that conjugate **I** does not entirely represent a monovalent species.

SPR spectroscopy for multivalent vancomycin interaction. SPR spectroscopy is a real-time kinetic method that allows the measurement of the on-rate constant (k_{on}), the off-rate constant (k_{off}), and equilibrium dissociation constant K_D (= k_{off}/k_{on}) for receptor−ligand interactions occurring on the surface.[24,25,31,57,58] It is important, in particular, for studying multivalent interactions, including those for vancomycin.[24,25,59] In this study, we employed SPR spectroscopy to determine the binding constant K_D for dendrimer-based multivalent vancomycin conjugates to the cell wall ligands immobilized on the chip surface as a model for the bacterial cell surface. The model surface was prepared by utilizing each CM5 sensor chip which was treated to present N^{α}-Ac-Lys-(D)-Ala-(D)-Ala or N^{α}-Ac-(D)-Ala-(D)-Lac as the cell wall precursor on the surface, each representing a vancomycin-susceptible and vancomycin-resistant cell wall model, respectively.[24,25] Such a peptide-presenting chip was prepared typically following a *N*-(3-dimethylaminopropyl)-*N*′-ethylcarbodiimide (EDC)-based amide coupling method as described previously[31,58] at a surface peptide density of 0.12 ng/mm^2 (equivalent to 2.2 × 10^{11} molecules/mm^2).[31,58]

Vancomycin-Susceptible Cell Wall Model. Dose-dependent binding sensorgrams for vancomycin to the (D)-Ala-(D)-Ala surface are shown in Figure 3A. Scatchard analysis of the SPR binding data provides a K_D value of 9.5 × 10^{-7} M, an affinity close to the value found in the literature ($K_D \approx 10^{-6}$ M),[25] demonstrating the susceptibility of the synthetic cell wall ligands to vancomycin binding. A fully acetylated G5 PAMAM, a negative control dendrimer without vancomycin attached, was tested for its binding but did not show any response to the (D)-Ala-(D)-Ala surface when otherwise measured under comparable conditions (Supporting Information, Figure S6). These data are supportive of the specificity of the cell wall model to vancomycin.

SPR binding studies were then performed for three representative vancomycin conjugates—**II** Ac-G5-(V)$_{2.3}$, **IV** Ac-G5-(V)$_{5.8}$, and **VI** GA-G5-(V)$_{6.0}$—each selected to address the effects of vancomycin valency and of dendrimer surface charge (Figure 3, S6). First, the SPR sensorgrams obtained for each conjugate illustrate the concentration-dependent binding kinetics at the range of concentrations as low as 2 nM at which free vancomycin shows no detectable response. The results for each conjugate **II**, **IV**, and **VI** suggest almost no evidence for nonspecific binding by the conjugates as illustrated by conjugate **IV**. Conjugate **IV** binds to the surface of flow cell 1, the bacterial cell model that presents (D)-Ala-(D)-Ala peptide precursors (specific binding), but does not bind to the surface of flow cell 2, the reference surface that does not present this cell wall peptide (nonspecific binding; Supporting Information, Figure S6). The result suggests binding specificity

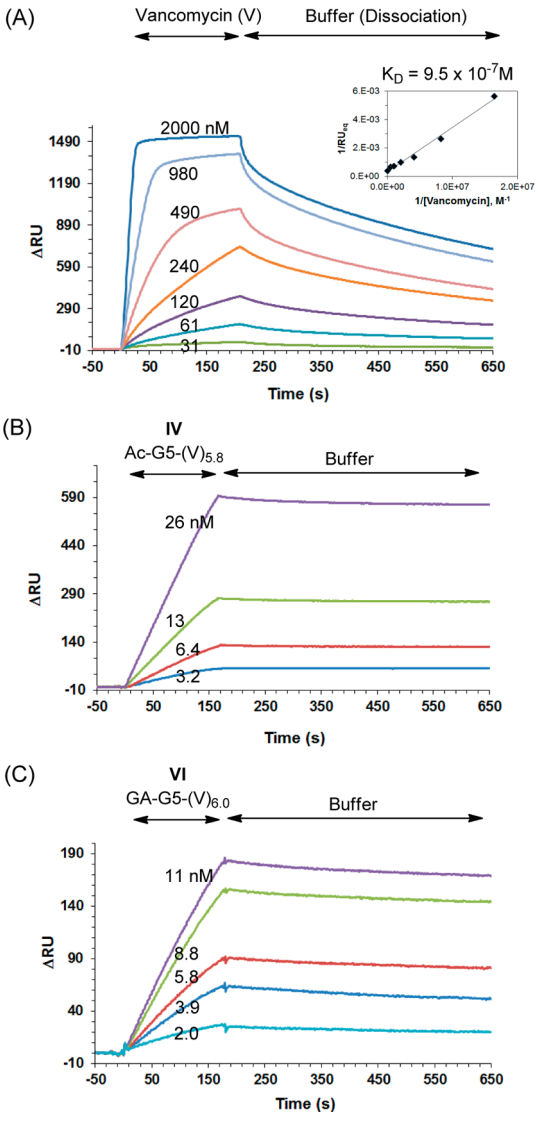

Figure 3. Surface plasmon resonance (SPR) studies for the binding kinetics of vancomycin (A), and the vancomycin-presenting PAMAM dendrimers, IV Ac-G5-(V)$_{5.8}$ (B) and VI GA-G5-(V)$_{6.0}$ (C), to the vancomycin-susceptible bacterial cell wall model. The model is made by immobilization of N^{α}-Ac-Lys-(D)-Ala-(D)-Ala peptide molecules on the CM5 sensor chip. The concentrations of vancomycin and its dendrimer conjugates injected are indicated in the overlay of the sensorgrams. The inset (A) is the Scatchard plot derived from the SPR data and used to determine the dissociation constant (K_D) of vancomycin.

of **IV** to this cell wall model. Each sensorgram acquired by conjugate **IV** shows binding kinetics characterized by an extremely slow dissociation-rate (almost permanently bound)—a hallmark of tight multivalent binding, as reported in other vancomycin-based multivalent systems.[21,24,25]

To determine the dissociation constant K_D for **IV**, we analyzed each sensorgram by a fitting analysis based on the Langmuir binding isotherm, as described elsewhere.[60] Despite the high level of uncertainty associated with such extremely slow dissociation, we were able to extract estimated values for its k_{off}

TABLE 2. Rate Constants and Equilibrium Dissociation Constants K_D for Binding Kinetics of G5-(V)$_n$ to the Bacterial Cell Wall Model As Determined by Surface Plasmon Resonance (SPR) Spectroscopy[a]

	k_{on} (M^{-1} s^{-1})	k_{off} (s^{-1})	K_D (M)[b]	β[d,e]
		(D)-Ala-(D)-Ala Surface (Vancomycin-Susceptible Cell Wall Model)		
vancomycin			9.5×10^{-7} (1.1×10^{-6})[25,c]	1
II Ac-G5-(V)$_{2.3}$	$1.5(\pm1.1) \times 10^5$	$4.5(\pm2.6) \times 10^{-4}$	$3.4(\pm1.9) \times 10^{-9}$	280 (122)
IV Ac-G5-(V)$_{5.8}$	4.5×10^5	$4.4(\pm1.3) \times 10^{-5}$	$2.5(\pm2.0) \times 10^{-10}$	3800 (655)
VI GA-G5-(V)$_{6.0}$	$6.7(\pm3.7) \times 10^5$	$3.6(\pm1.9) \times 10^{-4}$	$5.4(\pm0.6) \times 10^{-10}$	1759 (293)
		(D)-Ala-(D)-Lac Surface (Vancomycin-Resistant Cell Wall Model)		
vancomycin			1.5×10^{-3} (1.7×10^{-3})[24,c]	1
I Ac-G5-(V)$_{1.2}$	$9.8(\pm7.1) \times 10^4$	$6.6(\pm5.1) \times 10^{-4}$	$7.1(\pm2.7) \times 10^{-9}$	2.1×10^5 (1.8×10^4)
II Ac-G5-(V)$_{2.3}$	3.2×10^5	$4.1(\pm1.3) \times 10^{-4}$	8.1×10^{-9}	1.9×10^5 (8.1×10^4)
III Ac-G5-(V)$_{3.5}$	6.4×10^5	$4.5(\pm2.7) \times 10^{-4}$	$2.0(\pm1.8) \times 10^{-9}$	7.5×10^5 (2.1×10^5)
IV Ac-G5-(V)$_{5.8}$	6.9×10^5	$2.9(\pm0.4) \times 10^{-4}$	1.7×10^{-9}	8.8×10^5 (1.5×10^5)
VI GA-G5-(V)$_{6.0}$	$1.8(\pm1.7) \times 10^6$	$2.8(\pm1.5) \times 10^{-3}$	3.4×10^{-9}	4.4×10^5 (7.4×10^4)

[a] The model surface includes the vancomycin-susceptible, and vancomycin-resistant model, each prepared by immobilization of either the N^{α}-Ac-Lys-(D)-Ala-(D)-Ala peptide or N^{α}-Ac-Lys-(D)-Ala-(D)-Lac peptide on the surface of the sensor chip. [b] Each dissociation constant K_D ($= k_{off}/k_{on}$) is not derived directly from the pair of mean k_{off} and k_{on} values as given in the table. Rather, it represents a mean value calculated by averaging a set of K_D values, each calculated from an individual pair of k_{off} and k_{on} values determined per injection concentration. At least four different concentrations were used for the calculation, each run in duplicate per concentration. The number within parentheses refers to the standard error of the mean (SEM), and unless noted specifically, the standard error for each K_D value is within 2-fold variation. [c] Determined by Scatchard analysis. [d] β = Multivalent binding enhancement = $K_D^{vancomycin} \div K_D^{G5\text{-}(V)n}$ where $K_D^{vancomycin}$ and $K_D^{G5\text{-}(V)n}$ refer to the dissociation constants determined for vancomycin and G5-(V)$_n$ conjugates **I**–**IV** and **VI**, respectively. [e] The value within parentheses refers to the valency-corrected value ($= \beta \div n$).

($\leq 4.4 \times 10^{-5}$ s^{-1}) and k_{on} (4.5×10^5 M^{-1} s^{-1}), and, as a result, its K_D value ($\leq 2.5 \times 10^{-10}$ M). We also analyzed SPR sensorgrams for two other conjugates, **II** and **VI**, in a similar manner. Each of these conjugates showed a (sub)nanomolar K_D value as summarized in Table 2. The K_D values determined for **II**, **IV**, and **VI** suggest their binding avidity enhanced by a factor of 280–3800 (multivalent binding enhancement $\beta = K_D^{mono} \div K_D^{multi}$) relative to the free vancomycin molecule (K_D = 950 nM). Even the divalent conjugate **2** Ac-G5-(V)$_2$ shows a K_D value of 3.4 nM, an avidity value that still provides a β value of 280 over vancomycin. We also compared the avidity values between the two conjugates **IV** and **VI**, each having the same mean valency of vancomycin but presented on a different dendrimer surface, either neutral or negatively charged surface, respectively. Only a slight difference was observed, suggesting that the avidity may have already reached a maximal level at a lower valency (cf., **II**), and/or the effect of the surface charge might be minimal.

The SPR analysis shows that such improved avidity by each conjugate is attributed primarily to the slower off-rate (k_{off}). This observation fully supports the established hypothesis that complete dissociation of a multivalent species occurs very slowly because all of the individual binding interactions have to dissociate simultaneously from the surface.[32,61,62] Altogether, the SPR study performed on the vancomycin-susceptible cell wall model suggests that the avidity by the vancomycin conjugates is enhanced by two to three orders of magnitude, relative to the micromolar affinity of free vancomycin. It strongly validates the hypothesis of targeting bacterial cells by using a vancomycin-presenting dendrimer platform.

Vancomycin-Resistant Cell Wall Model. We extended the SPR study to examine another cell wall model that mimics the vancomycin-resistant bacterial cell. In this model, (D)-Ala-(D)-Lac peptides are immobilized in lieu of the (D)-Ala-(D)-Ala residue as the cell wall precursor, and the resulting surface shows reportedly ~1000-fold reduction in affinity to free vancomycin ($K_D \approx 10^{-3}$ M).[24,29] We performed dose-dependent binding experiments for vancomycin to the (D)-Ala-(D)-Lac surface as shown in Figure 4A. In contrast to the susceptible model surface, vancomycin shows very low responses, even when injected at much higher concentrations. The Scatchard analysis (inset) of its binding responses provides a K_D estimate of 1.5×10^{-3} M, a value close to the value in the literature ($K_D = 1.7 \times 10^{-3}$ M).[24] This control experiment confirms that this chip mimics the vancomycin-resistant cell wall model by showing only millimolar affinity to free vancomycin.

We then investigated whether multivalent ligand presentation enables the generation of a high avidity species that binds tightly to the vancomycin-resistant surface and improves the poor affinity of free vancomycin.[31,32,34,35] SPR experiments were performed for a series of vancomycin conjugates, **I**–**IV** Ac-G5-(V)$_n$ and **VI** GA-G5-(V)$_6$, each selected to cover a range of valencies and to address the difference in surface charge (Figure 4, S7). The experiments showed remarkably strong binding responses to the surface in a concentration-dependent manner, even at low nanomolar concentrations. Compared to the vancomycin-sensitive surface (Figure 3), the dissociation kinetics of the higher-valent conjugates **IV** and **VI** is characterized by slightly faster dissociation (k_{off}) by approximately an order of magnitude (Table 2). Despite such

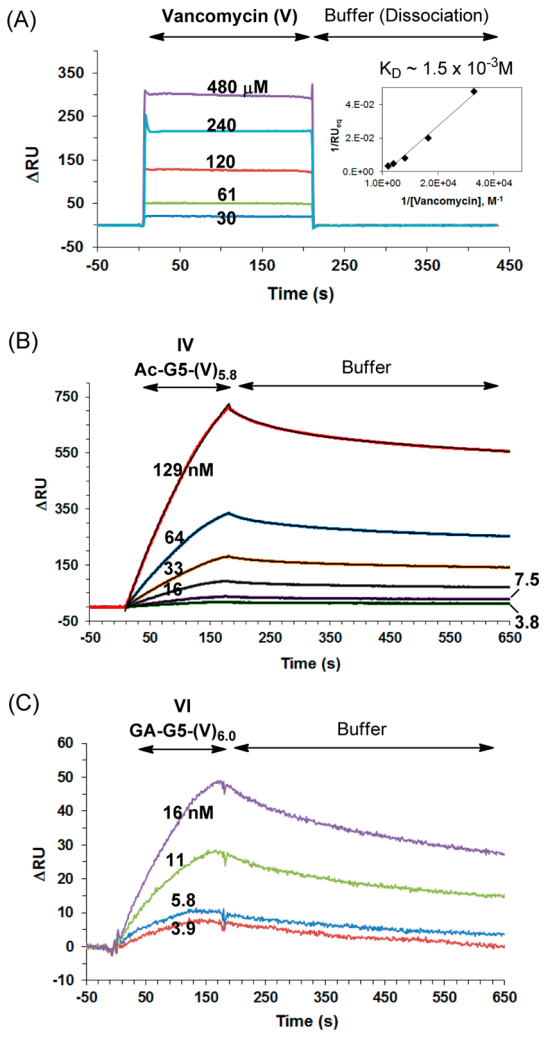

Figure 4. Surface plasmon resonance (SPR) studies for the binding kinetics of vancomycin, and the vancomycin-presenting PAMAM dendrimers G5-(V)$_n$ to the vancomycin-resistant bacterial cell wall model. The model is made by immobilization of N^{α}-Ac-Lys-(D)-Ala-(D)-Lac peptide molecules on the CM5 sensor chip. SPR sensorgrams for vancomycin (A), IV Ac-G5-(V)$_{5.8}$ (B), and VI GA-G5-(V)$_{6.0}$ (C) are acquired at the range of the concentrations as indicated. The inset (A) is the Scatchard plot derived from the SPR data in order to determine the K_D value of vancomycin. Fitting curves are illustrated for those sensorgrams (B) as overlaid in black lines.

differences, each of these conjugates still showed a K_D value in the low nanomolar range (K_D = *ca.* 2−3 nM). This avidity constant represents an enhancement by more than 5 orders of magnitude relative to the millimolar affinity of the free vancomycin molecule. The lower-valent conjugates **I** and **II** also showed K_D values of 7−8 nM, which is slightly lower in avidity than those of the higher-valent conjugates, **III**−**VI**.

Given the low valency (n = 1.2) of conjugate **I** Ac-G5-(V)$_{1.2}$, its K_D value is still remarkably low at the nanomolar range and its avidity enhancement is comparable to that displayed by each higher-valent conjugate, **II**−**VI**. We hypothesize that such a high avidity constant exhibited by **I** is not due to tight binding by its monovalent conjugate but reflects that of the distribution of its population. As discussed earlier in the Poissonian distribution of **I** (Figure 2), only 36% of the dendrimer species in this sample represent the monovalent dendrimer (n = 1). Approximately the same fraction (34%) of the dendrimer populations belongs to the multivalent species ($n \geq 2$), and such a fraction might contribute to the binding responses observed for **I**.

To better understand the binding kinetics displayed by the current stochastically prepared multivalent dendrimers, we analyzed each sensorgram (adsorption, desorption) by fractional analysis for conjugates **I**−**IV** Ac-G5-(V)$_n$, each measured at the identical concentration 50 nM (Figure 5). First the maximal level of adsorption (RU_A) observed by each conjugate is ordered as follows: **IV** > **III** > **II** > **I** (Figure 5B). Such differences in adsorption are not simply explained by their equilibrium association constants ($K_A = K_D^{-1}$: **IV** ≈ **III** > **II** ≈ **I**). Interestingly, it is better correlated with the fraction of multivalent species ($n \geq 2$) distributed in each conjugate (Figure 2), suggesting that these multivalent species are significantly responsible for the adsorption to the surface. In contrast, the separate desorption analysis performed for each dissociation curve shows almost no difference in fractional desorption between the four sensorgrams. This analysis is illustrated by a plot of the off-rate constant (k_{off}, Table 2) and the level of fractional desorption (= RU_D/RU_A) for each conjugate (Figure 5C). It suggests that those dendrimer populations bound at the end of each association phase are likely represented by tight binding species, each having a valency of $n \geq 2$. This fractional binding is supported by (sub)nanomolar dissociation constants associated with divalent and trivalent vancomycin species reported by Whitesides, *et al.*[22,24,25]

Another aspect to consider that is important for understanding the mechanistic basis of multivalent association is the effective molarity of surface ligands available for binding. Effective molarity (M_{eff}) or effective concentration—a concept pioneered by Jencks, *et al.*[63] in the analysis of intramolecular catalysis—refers to the ratio of the equilibrium constant of an intramolecular association to that of an analogous intermolecular association.[23,64−66] In our system, we define M_{eff} as $[(K_D^{vancomycin}) \times (K_D^{vancomycin})]/[(K_{D1}^{G5\text{-}(V)n}) \times (K_{D2}^{G5\text{-}(V)n})] \approx (K_D^{vancomycin})^2/(K_D^{G5\text{-}(V)n})$ as described in the literature[23,62−64] where $K_{D1}^{G5\text{-}(V)n}$ and $K_{D2}^{G5\text{-}(V)n}$ refer to the first and second dissociation constant of a divalently bound conjugate G5-(V)$_n$, respectively (for definition of $K_D^{vancomycin}$ and $K_D^{G5\text{-}(V)n}$, see Table 2 footnotes). We characterize M_{eff} as an effective local concentration of surface ligands that contribute to the second binding event. Values of M_{eff} calculated for conjugates **II**, **IV**, and **VI** are ~2.7 × 10^{-4}, 3.6 × 10^{-3}, and 1.7 × 10^{-3} M, respectively, when applied for their

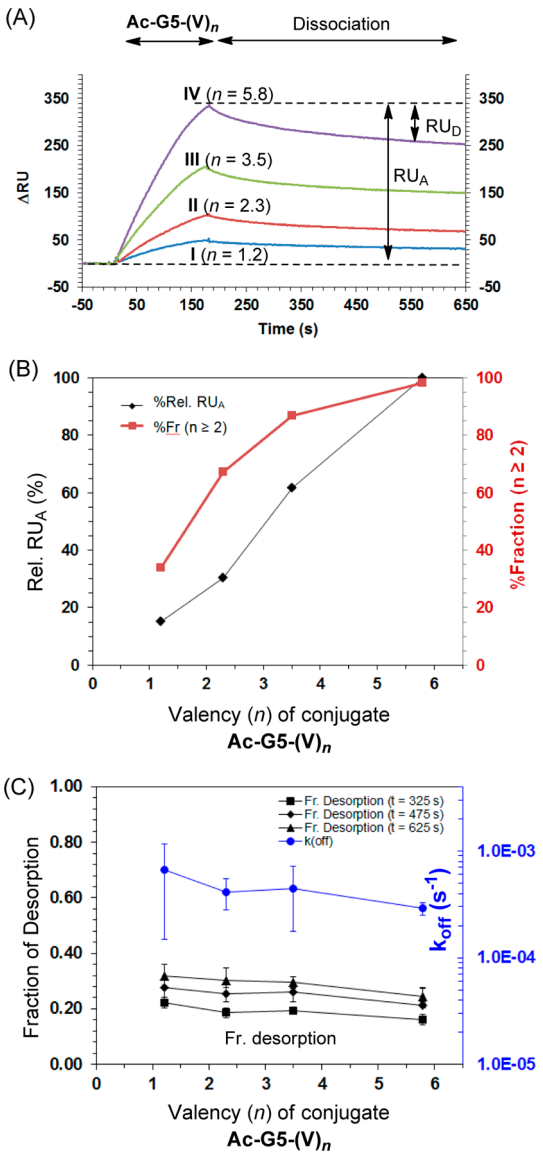

Figure 5. (A) An array of selected SPR sensorgrams for Ac-G5-$(V)_n$ binding to (D)-Ala-(D)-Lac peptide molecules on the surface, each acquired at the identical concentration including I Ac-G5-$(V)_{1.2}$ (50 nM), II Ac-G5-$(V)_{2.3}$ (50 nM), III Ac-G5-$(V)_{3.5}$ (51 nM), and IV Ac-G5-$(V)_{5.8}$ (50 nM). (B) Relative adsorption (RU_A) of Ac-G5-$(V)_n$ and fraction (%) of multivalent populations ($n \geq 2$; inset of Figure 2). Relative adsorption is defined as RU_A (conjugate) relative to RU_A (IV; 100%). (C) Comparison of off-rate constant k_{off} (Table 2) and fractional desorption of Ac-G5-$(V)_n$ as a function of valency (n). The fractional desorption is defined as the level of the dendrimer desorbed (RU_D) relative to the level of the dendrimer adsorbed (RU_A) as illustrated for the conjugate IV. Each value of the RU_A and RU_D was calculated as the mean value from at least six different injection concentrations per conjugate at the specific time point indicated. Each error bar indicates the standard error of the mean (SEM).

adsorption to the vancomycin-susceptible surface presenting (D)-Ala-(D)-Ala ligand molecules. This analysis indicates that the M_{eff} values of the peptide ligand are two to three orders of magnitude higher than the dissociation constant of the same ligand to vancomycin ($K_D = 9.5 \times 10^{-7}$ M). Thus we assume that such a

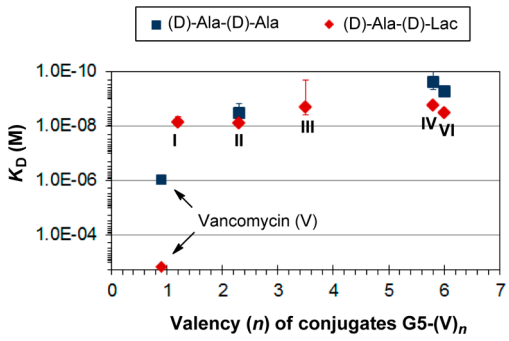

Figure 6. Equilibrium dissociation constants (K_D, M) of G5-$(V)_n$ I–IV, VI determined by the SPR binding to the cell wall model made of either (D)-Ala-(D)-Ala or (D)-Ala-(D)-Lac peptides as a function of valency (n). The K_D values for free vancomycin are placed arbitrarily around n = 0.9 as the reference point indicative of the affinity constant for its monovalent association. Each error bar indicates the standard error of the mean (SEM).

difference is large enough to explain the tight adsorption of these conjugates. We also estimated M_{eff} values for the other vancomycin-resistant surface that presents (D)-Ala-(D)-Lac ligand molecules. The corresponding values of M_{eff} for conjugates **I**–**VI** lie in the range of ~280 to 1300 M. Such ligand molarities are implausibly high, but support the high avidity adsorption of the conjugates to the drug-resistant surface because the ligand concentrations are extremely high and far above the dissociation constant of vancomycin to the same ligand ($K_D \approx 1.5 \times 10^{-3}$ M).

In summary, we performed the SPR study to determine the equilibrium dissociation constants K_D of G5-$(V)_n$ **I**–**IV** and **VI** to the cell wall model made of either (D)-Ala-(D)-Ala or (D)-Ala-(D)-Lac peptide precursor, as summarized in Figure 6. This study demonstrates the effectiveness of the multivalent strategy for achieving high avidity binding to the cell wall models, including the vancomycin-resistant surface, and therefore suggests its capability for effective targeting of bacterial cells.

Confocal microscopy. We performed confocal microscopy to determine whether the SPR binding study for cell wall models is translatable to bacterial cells (Figure 7). We treated Gram-positive bacteria *Staphylococcus aureus* with fluorescein-labeled vancomycin conjugates **VIII** DTPA-G5-$(V)_{6.1}$-$(Fl)_{3.9}$ and **IX** Ac-G5-$(V)_{6.3}$-$(FITC)_{1.8}$, as shown in Figure 7. The treatment resulted in punctate green fluorescence (Figure 7A,B). Since this green fluorescence comes from the dye on the conjugate, each image indicates binding of the dendrimer to the cell surface. In contrast, cells treated with a nontargeted control dendrimer, GA-G5-(FITC) (Figure 7C) or Ac-G5-(FITC) (not shown), showed no noticeable green fluorescence on the cells. Each sample of the treated cells was also stained for DNA using Syto59, which confirmed that the green spots associated with the dendrimers were in fact associated with intact cells rather than cellular debris. Interestingly, treatment of

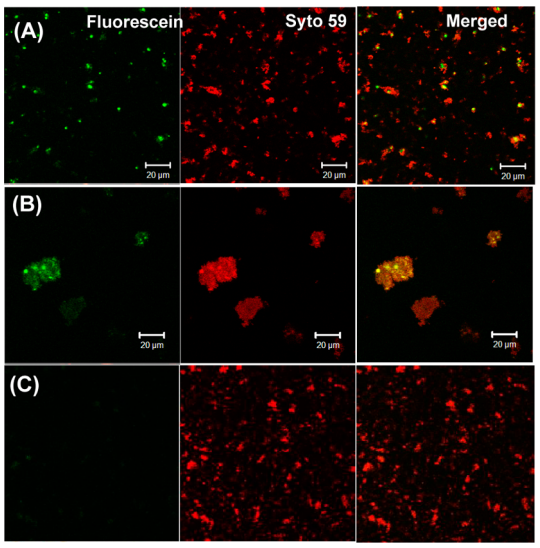

Figure 7. Confocal images of Gram-positive bacterial cells (*Staphylococcus aureus*: ATCC 4012) treated with VIII DTPA-G5-$(V)_{6.1}$-$(FI)_{3.9}$ (A), IX Ac-G5-$(V)_{6.3}$-$(FITC)_{1.8}$ (B), or GA-G5-(FITC) as a nontargeted control dendrimer (C). The cells were incubated with each of the dendrimers (86 μM), washed, and stained with Syto 59, a cell-permeable fluorescent molecule (emission wavelength = 645 nm; red) that intercalates into the DNA molecule inside the nucleus. Adsorption of the dendrimer nanoparticles to the bacterial cells is indicated by the green fluorescence (fluorescein; emission wavelength = 520 nm) in those cells treated with VIII or IX, but not by the negative control GA-G5-(FITC). The fluorescent objects in panel B show much larger images than as expected for individual bacterial cells and are attributable to the bacterial aggregates, possibly due to the cross-linking by the vancomycin-conjugated multivalent dendrimers (scale bar = 20 μm).

the cells with **IX** Ac-G5-$(V)_{6.3}$-$(FITC)_{1.8}$ resulted in large clumps or aggregates of bacterial cells. This is most likely due to the cross-linking of multiple bacterial cells, mediated by multiple vancomycin molecules on each dendrimer.

Bacterial Cell Lysis. We investigated whether the binding of the vancomycin-conjugated dendrimer to the bacterial membrane causes bacterial cell lysis. Cell lysis constitutes one of the mechanisms for killing bacteria,[67] though lack of lysis does not necessarily preclude the therapeutic effectiveness of tested conjugates.[68] On the other hand, the lack of such a mechanism would be more desirable for the diagnostic applications that aim for bacterial detection, isolation, and enumeration of whole cells. To determine the degree of cell lysis, we employed a turbidity assay. This assay quantitates the bacterial population in a culture by measuring the optical density (OD at 650 nm), and the cell populations are correlated with the degree of lysis.[67,68] Effects of the conjugates **I**–**VI**, **VIII**, **IX** on the cell growth rate were determined using the same Gram-positive strain *Staphylococcus aureus* and were presented as a function of the inhibitor concentration (Figure 8, S8A). As illustrated by conjugates **VIII** and **IX** in Figure 8, the bacterial cultures exposed to the

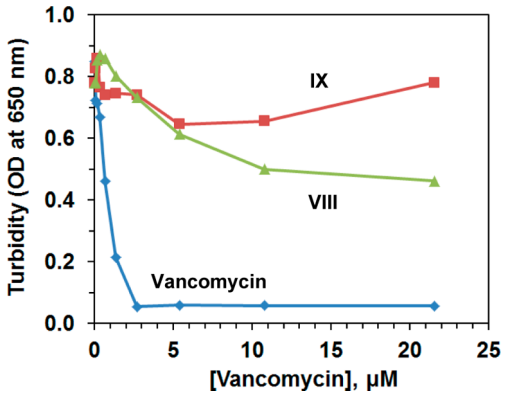

Figure 8. A turbidity assay to determine the ability to cause cell lysis by vancomycin-conjugated dendrimers VIII DTPA-G5-$(V)_{6.1}$-$(FI)_{3.9}$ and IX Ac-G5-$(V)_{6.3}$-$(FITC)_{1.8}$ against Gram-positive bacterial cells (*Staphylococcus aureus*). Test concentrations for each conjugate are given on the molar basis of the vancomycin molecules in the solution, [vancomycin] = $n \times$ [G5-$(V)_n$].

vancomycin conjugate showed much less change in optical density than free vancomycin, which decreased the optical density to the background level at $\geq$0.1 μM. However, certain differences in the lysis activity were also seen among the conjugates. Conjugate **VIII** shows a greater reduction in optical density than **IX**. Other conjugates tested **I**–**VI** showed no significant or only small changes in the turbidity assay at the high doses of $\leq$20 μM (Figure S8A).

This assay result suggests that the vancomycin-conjugated dendrimer has low activity for causing bacterial cell lysis despite its adsorption to the cell membrane, as indicated by the confocal images. Such a mode of activity is not unique to the current vancomycin-conjugated dendrimers but is also reported for vancomycin-derived glycopeptide antibiotics including telavancin (Vibativ) that shows potent bactericidal activity without causing cell lysis.[49,68] Given the complexities of the interactions between PAMAM dendrimers and bacterial membranes reported earlier,[69] there should be other factors that limit membrane penetration and cell lysis, such as the nanometer size of the conjugate particle ($d \geq$ 5.4 nm) and the polyionic nature of the surface. We believe that such lack of cell lysis provides a significant advantage for diagnostic purposes, as sensitive bacterial detection depends not only on its tight binding to the bacterial cell, but also on its ability to retain the intact cell for the entire duration of the assay.

Mammalian Cell Toxicity. In addition to the bacteria-targeted assays, we also investigated the effect of vancomycin-conjugated dendrimers to mammalian cells.[70,71] Human cervical KB cells and mouse melanoma B16–F10 cells were separately studied to evaluate the cytotoxicity of the representative conjugates **II**, **IX**, **VI**, and **VII** (Supporting Information, Figure S8).[71] As a reference, the positively charged G5-NH_2 showed a dose-dependent cytotoxicity apparently starting at

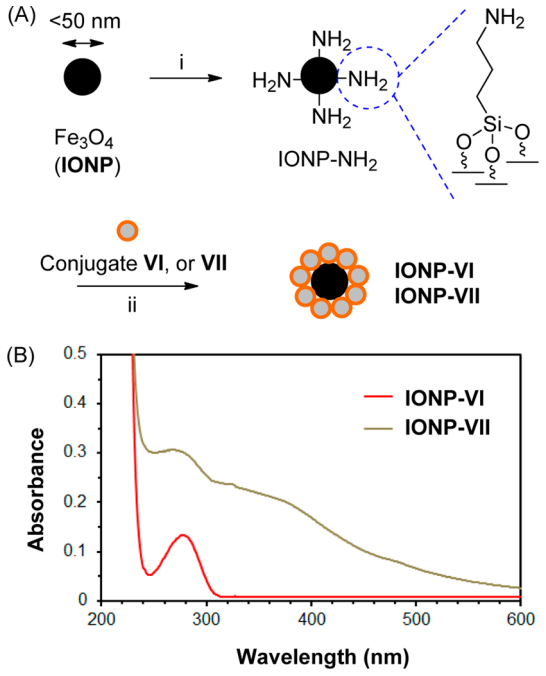

Scheme 2. Synthesis (A) and UV-vis spectra (B) of iron oxide (Fe_3O_4)-based nanoparticles IONP-VI and IONP-VII. Reagents and conditions: (i) $(MeO)_3Si(CH_2)_3NH_2$, AcOH (cat.), toluene, RT, 12 h; (ii) VI GA-G5-$(V)_{6.0}$ (for IONP-VI), or VII DTPA-G5-$(V)_{6.1}$ (for IONP-VII), EDC, NHS, DMF/DMSO (3:2), RT, 6 h. The size of those reacting nanoparticles is not drawn to scale. UV-vis spectra for IONP-VI and IONP-VII were obtained by suspending each sample in water at the vancomycin concentration of 13 μM and 44 μM, respectively.

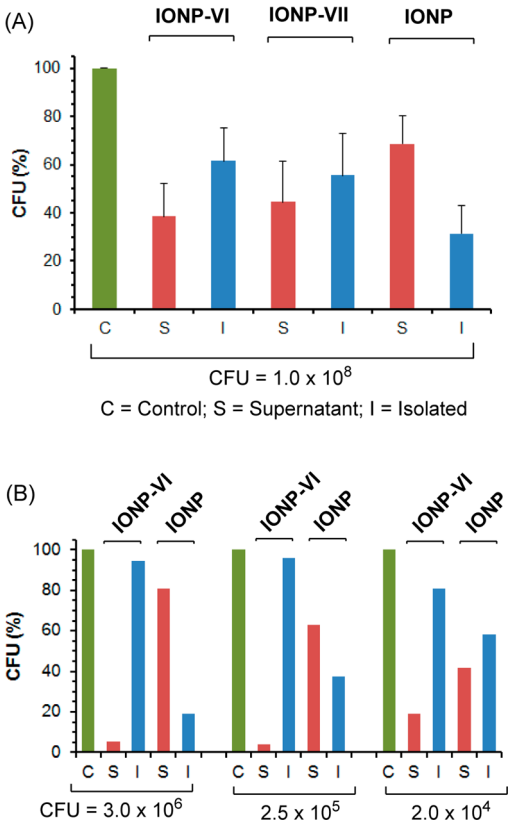

Figure 9. Magnetic isolation of Gram-positive bacterial cells (*Staphylococcus aureus*) by using cell wall-targeting magnetic nanoparticles IONP-VI and IONP-VII. Variable titers of bacterial cells were incubated with either IONP-VI, IONP-VII, or a control IONP (no dendrimer coated), each at 0.25 IONP mg per 1.0 $\times$ 10^8 CFU bacteria (A), and 2.0 $\times$ 10^4 – 3.0 $\times$ 10^6 CFU bacteria (B). Those bound with magnetic nanoparticles were isolated under the magnetic field. The level of the bacterial cells isolated (I) or retained in the supernatant (S) after each treatment was quantified by the cell culture assay, and expressed as % colony forming unit (CFU) relative to the control level (C; no treatment). The results are presented as mean $\pm$ standard error of the mean (SEM; 12–17%).

1000 nM, as reported earlier.[71] The vancomycin conjugates **II**, **IV**, and **VI** were not cytotoxic when tested under the otherwise identical conditions. Such a result, which is consistent with the relatively no cytotoxicity displayed by neutral or negatively charged dendrimers, suggests that further modifications made through vancomycin conjugation did not lead to any effect on cell growth. However, conjugate **7**, the surface of which is fully covered with metal-free DTPA groups, showed toxicity at 1000 nM as potent as G5-NH_2. Such growth inhibition is not understood at this time, but we speculate that this effect might be related to the high local concentration of the free DTPA group ($[DTPA]_{free} \approx$ 0.1 mM), a strong metal chelator which is linked to depletion of endogenous trace metals.[72,73]

Synthesis of Dendrimer-Coated IONP. After identification of the vancomycin-conjugated dendrimers that show high avidity to the bacterial surface, we explored the applicability of this dendrimer platform as laboratory and clinical tools that enable selective binding and isolating of bacteria. We investigated whether the bacteria-targeting technology can be combined with the speed and convenience provided by magnetic isolation technology. Two conjugates, **VI** GA-G5-$(V)_{6.0}$ and **VII** DTPA-G5-$(V)_{6.1}$, were selected for this purpose, and each was coupled with an iron oxide nanoparticle (IONP) to generate magnetic nanodevices (Scheme 2).

In the first step, IONP (Fe_3O_4; mean d < 50 nm) was treated with (3-aminopropyl)trimethoxysilane in order to chemically modify its surface to present primary amines (IONP–NH_2) that will serve as the chemical handle for dendrimer conjugation.[74] Each conjugate, **VI** or **VII,** was covalently attached to the IONP–NH_2 by an EDC-based amide coupling method, yielding **IONP-VI**, and **IONP-VII**, respectively. Each of these dendrimer-coated IONPs was characterized by UV–vis spectrometry, confirming the presence of a vancomycin conjugate (Scheme 2; λ_{max} = 282 nm). The conjugation efficiency of **VI** or **VII** to IONP was estimated by colorimetric analysis, which indicated that ~75% of the conjugates added in the reaction mixture were covalently attached.

Magnetic Bacterial Isolation. We tested the effectiveness of bacterial removal in aqueous samples by bacteria-targeting magnetic nanoparticles. The amount of bacteria was quantified both in the supernatant and

on IONPs by using a standard culture method[8] where aliquots of the supernatant and isolated IONPs were serially diluted and plated on agar plates to enumerate bacterial CFU. Figure 9 summarizes the results obtained by **IONP-VI** and **IONP-VII** for their ability to isolate *Staphylococcus aureus* bacterial cells from highly enriched bacterial samples (0.25 mg IONP per 10^4 – 10^8 CFU bacteria). The ratio of bacterial cells added per IONPs varied over 4 orders of magnitude in bacterial CFU and each of such bacterial titers was arbitrarily chosen to gauge the low range of the IONPs in the isolation of bacterial cells. Briefly, this procedure was performed in three steps: (i) incubation of bacteria inoculum with the IONPs, (ii) magnetic separation of bacteria adhered to IONPs from the supernatant, (iii) enumeration of bacterial CFU of the pellet by using the agar culture method.

First, at the highest bacterial titer (10^8 CFU; Figure 9A), an unmodified IONP which is the nontargeted control showed that about 69(±12)% of the bacteria remained in the supernatant relative to the level obtained by the IONP-free control, and therefore the bare IONP control showed the ability to capture ~31% of the bacteria added. This result is largely consistent with the conclusion reached about unmodified iron oxide particles that is reported elsewhere, that its ionic surface can promote nonspecific adhesion of bacterial cells primarily through electrostatic interactions.[75,76] In comparison, targeted experiments that were performed using both **IONP-VI** and **IONP-VII** showed 61(±14)% and 56(±17)% of bacterial isolation, respectively. Thus, each of these dendrimer-coated IONPs was able to capture bacterial cells at the efficiency ~2-fold greater than the nontargeted control. Such capturing capability appears to be compromised due to excess bacterial loads and indicates a maximal level of the bacteria to be captured per IONPs added.

Second, we compared the efficiency of bacterial capture by **IONP-VI** and IONP at the lower range of bacterial titers (10^4–10^6 CFU; Figure 9B). Targeted experiments using **IONP-VI** showed 81–96% of bacterial isolation, an efficiency greater than those obtained in the higher bacterial titer (Figure 9A). Thus, the results support that the average level of bacterial capture is correlated with the bacterial load per targeted IONPs. Such results from the targeted **IONP-VI** are greater than those from the nontargeted IONP which showed approximately 20–60% bacterial isolation under the same conditions. Interestingly, the efficiency of the bare IONP rapidly deteriorated in response to the increase in bacterial load, suggesting that its capture capability is limited and easily saturable. In summary, the experiments illustrate the practicality of magnetic NPs coated with bacteria-targeting dendrimers for rapid bacterial isolation in aqueous samples.

CONCLUSIONS

We described a new class of dendrimer-vancomycin nanoconjugates designed for bacteria targeting. The core of this nanotechnology is based on a multivalent strategy applied for PAMAM dendrimer conjugated with vancomycin as a bacteria-targeting agent. SPR spectroscopy showed that these vancomycin conjugates bind tightly to two synthetic models of the bacterial cell wall at (sub)nanomolar dissociation constants, indicating an avidity enhancement by four to five orders of magnitude over free vancomycin. In particular, this SPR study provides evidence that these multivalent species still bind tightly to a vancomycin-resistant surface which otherwise shows only weak (millimolar) affinity to vancomycin. As a practical application, this study demonstrates that bacteria-targeted dendrimers could be used for fabrication of magnetic NPs, and the resultant hybrid NPs open a convenient route for magnetic isolation and enumeration of bacteria. Although a variety of bacteria-targeted nanotechnologies have been actively pursued,[9,20,21,27] we believe that this specific dendrimer platform represents a significant advancement in nanotechnology with inherent modularity providing many options for rapid and portable monitoring and removal of bacterial contaminants in biological samples. Future efforts will focus on exploring and enhancing the scope of such magnetic applications.

EXPERIMENTAL SECTION

Materials and Methods. Unless described as below, most experimental details for conjugate synthesis and instrumental analysis are provided in the Supporting Information (Page S2–S3) and references cited therein.[15,39,53,77]

Representative Synthetic Methods for G5-(Vancomycin)$_n$ (Scheme 1). *Preactivation of Vancomycin.* To a solution of vancomycin hydrochloride hydrate (64 mg, 43 μmol) dissolved in a mixture of anhydrous DMSO (2 mL) and DMF (1 mL) was added *N,N*-diisopropylethylamine (15 μL, 86 μmol), 1-hydroxybenzotriazole hydrate (HOBt, 6.6 mg, 49 μmol), and then benzotriazol-1-yloxytripyrrolidinophosphonium hexafluorophosphate (PyBOP; 23 mg, 44 μmol) in a sequence. After stirring for 40 min at room temperature, this solution was divided into three aliquots: 0.66 mL (aliquot A), 1.05 mL (aliquot B), and 1.29 mL (aliquot C). Each of the three aliquots (containing the activated ester of vancomycin) was used immediately for conjugation to G5 PAMAM dendrimer (G5-NH_2) as follows.

Conjugates III–V Ac-G5-(V)$_n$ (n = 3.5, 5.8, 8.3). Typically, each aliquot was added to a rapidly stirred solution of G5-NH_2 (MW = 26700 g mol^{-1}; 50 mg, 1.87 μmol) dissolved in methanol (12 mL) at the specific molar ratio of vancomycin to the dendrimer ([vancomycin]/[G5-NH_2] = 5, 8, 10). Then each mixture was stirred for 5 h at room temperature prior to the addition of *N,N*-diisopropylethylamine (59 μL, 339 μmol) followed by the addition of acetic anhydride (16 μL, 170 μmol). The final reaction mixture was stirred for an additional 1 h at room temperature,

and concentrated *in vacuo*. The residue was diluted with 20 mL of phosphate-buffered saline (PBS, pH 7.4), loaded into cellulose membrane dialysis tubing (MWCO 10 kDa), and dialyzed against PBS (2 L × 2), and deionized water (2 L × 2) over 2 days. The purified solution in each of the dialysis bags was collected and lyophilized to afford Ac-G5-$(V)_n$ as white fluffy solid: 65 mg (from aliquot A), 75 mg (aliquot B), 87 mg (aliquot C). The purity of each conjugate Ac-G5-$(V)_n$ was assessed by an analytical HPLC method: t_r = 7.75−7.76 min (n = 3.5, 5.8, 8.3), purity ≥ 99%. The number (n) of vancomycin molecules linked to each dendrimer conjugate Ac-G5-$(V)_n$ was determined on a mean basis by the analysis of UV−vis and MALDI mass spectral data: n = 3.5 (aliquot A condition); n = 5.8 (aliquot B condition); n = 8.3 (aliquot C condition). MALDI TOF mass spectrometry (m/z, g mol^{-1}): 32300 (**III**); 36300 (**IV**); 37500 (**V**). UV−vis for Ac-G5-$(V)_n$ (PBS, pH 7.4): 282 nm (λ_{max}). Each conjugate was also characterized by the GPC method to determine its molecular weights (weight-averaged M_w and number-averaged M_n) and a polydispersity index value (PDI = M_w/M_n). **III** Ac-G5-$(V)_{3.5}$: M_w = 30700 g mol^{-1}, PDI = 1.043. **IV** Ac-G5-$(V)_{5.8}$: M_w = 37800 g mol^{-1}, PDI = 1.027. **V** Ac-G5-$(V)_{8.3}$: M_w = 33200 g mol^{-1}, PDI = 1.032. Representative ^{1}H NMR data (500 MHz, D_2O; Supporting Information, Figure S4) for **V** Ac-G5-$(V)_{8.3}$: δ 7.8−7.6 (br (broad) s (singlet)), 7.4 (br s), 7.2−6.9 (br peak), 6.6−6.5 (br s), 6.3 (br s), 5.7 (br s), 5.5 (br s), 5.3 (br s), 5.2 (br s), 4.6 (br peak), 4.3−4.1 (br peak), 3.8−3.7 (br peak), 3.3−3.1 (br s; dendrimer), 3.0−2.2 (multiple peaks; dendrimer), 1.9 (s; *N*-Ac, dendrimer), 1.7 (br s), 1.6−1.5 (br peak), 1.4−1.2 (br peak), 0.9 (br s) ppm.

Synthesis of Dendrimer-Coated IONP-VI and IONP-VII (Scheme 2). *Amine-terminated IONP.* Iron oxide nanoparticles (Fe_3O_4, <50 nm; 3 g) were placed in a glass flask containing toluene (100 mL). To this suspension was added a catalytic amount of acetic acid (0.1 mL), and then followed by the addition of (3-aminopropyl)trimethoxysilane (APMS) while shaking the mixture mechanically. After shaking the mixture overnight at room temperature, the iron oxide particles were collected by centrifugation (4500 rpm). It was rinsed four times with toluene, each time according to a rinsing protocol that comprises (i) suspension in toluene (50 mL), (ii) sonication (30 s), (iii) spinning (4500 rpm). Subsequently, drying under a nitrogen flow afforded APMS-coated iron oxide particles (3.25 g).

IONP-VI and IONP-VII. As a first step in coupling of vancomycin-conjugated dendrimer nanoparticles to the amine-terminated IONPs prepared above, each dendrimer conjugate was prepactivated by an EDC method as follows. To a solution of **VI** GA-G5-$(V)_6$ (MW = 37100 g mol^{-1}) or **VII** DTPA-G5-$(V)_{6.1}$ (MW = 62500 g mol^{-1}), each (10 mg) dissolved in a mixture of DMSO (2 mL) and DMF (3 mL), was added 4-dimethylaminopyridine (DMAP; 50 mol equiv to dendrimer), *N*-hydroxysuccinimide (NHS; 100 equiv), and finally *N*-(3-dimethylaminopropyl)-*N*′-ethylcarbodiimide hydrochloride (EDC; 100 equiv). After stirring each reaction mixture at room temperature for 12 h, the activated dendrimer conjugate reacted with APMS-coated IONP (300 mg) by adding the IONP to the conjugate solution. The mixture was mechanically shaken at room temperature for 6 h, and then diluted with water (1 mL) prior to the addition of a second portion of EDC (100 mg each). The final mixture was shaken at room temperature for an additional 12 h. Isolation of **IONP-VI** or **IONP-VII** started with dilution of each reaction mixture with 14 mL of water and followed by centrifugation at 4500 rpm. A dark brown pellet was collected by carefully decanting the supernatant, and it was resuspended in water (14 mL). After a short period of sonication (30 s), the mixture was centrifuged and the pellet was collected. This rinsing process continued but by using 70% aq EtOH (14 mL). Each pellet (**IONP-VI** or **IONP-VII**) was collected and stored as a suspension in 70% aq EtOH (~25 mg/mL): UV−vis (70% aq EtOH), λ_{max} = 282 nm. The fraction of dendrimer conjugates **VI** (or **VII**) attached to IONP was estimated by a colorimetric analysis of unreacted dendrimer conjugates left in the supernatant using UV−vis spectrophotometry: Fr_{free} = $[conjugate]_{supernatant} \div [conjugate]_{added}$; $Fr_{attached} = (1 - Fr_{free}) \approx 0.75$. This fractional analysis was used to calculate the ratio of the conjugate attached to IONP on a percent weight basis: $(wt_{conjugate} \div wt_{IONP}) \times 100 \approx 2.5\%$.

SPR Spectroscopy. SPR experiments were carried out on a Biacore X instrument (Pharmacia Biosensor AB, Uppsala, Sweden) following the protocol, as reported elsewhere.[31,57,58] Cell wall models for Gram-positive bacteria were generated by immobilizing cell wall precursor peptides, either N^{α}-Ac-Lys-(D)-Ala-(D)-Ala (Sigma-Aldrich) or N^{α}-Lys-(D)-Ala-(D)-Lac (Bachem), to a CM5 sensor chip (Biacore). Thus each chip surface represents a vancomycin-susceptible or vancomycin-resistant cell wall model, respectively. As an illustration, the carboxymethylated dextran-coated layer of the chip was preactivated by injection (flow rate = 10 μL/min; volume = 50 μL) of a 1:1 mixture of EDC (0.4 M) and NHS (0.1 M), each dissolved in H_2O. Immediately after this preactivation step, each peptide solution prepared in H_2O (70 μL, 20 mg/mL, pH = 9−10) was injected for covalent attachment of the peptide to the dextran surface, followed by injection of ethanolamine (50 μL, 1 M, pH 8.0) to convert unreacted activated esters to neutral amides on the surface. The immobilization process resulted in a net increase in response unit (RU) of 120 (0.12 ng/mm^2 equivalent to ~2.2×10^{11} molecules/mm^2) for each peptide. A reference flow cell in each chip was then prepared in a similar way but without injecting the peptide. SPR studies were carried out by injecting an analyte solution, each prepared in HBS-EP buffer, at a flow rate of 20 μL/min for free vancomycin molecule as a positive control, or 10 μL/min for dendrimer conjugates G5-$(V)_n$. After each run, the surface of the chip was regenerated by repeated injections of an N^{α}-Ac-Lys-(D)-Ala-(D)-Ala solution (10 mg/mL) until the baseline of the sensorgram reached an initial level.

For kinetic analysis, each SPR sensorgram acquired from flow cell 1 (RU_1; peptide immobilized) was corrected for nonspecific binding by subtraction of the reference sensorgram from flow cell 2 (RU_2), as illustrated in Supporting Information, Figure S6 ($\Delta RU = RU_1 - RU_2$). Kinetic binding parameters, the on-rate (k_{on}), and the off-rate (k_{off}), were extracted by fitting each sensrogram separately using the Langmuir kinetic model, as described elsewhere.[31,57,60,78] Given the nature of dendrimer distribution associated with each conjugate, the fitting of each dissociation curve by employing a single exponential decay function was problematic. We assume that the decay curve represents a summation of two or more independent dissociation kinetics, each attributable to a group of dendrimer populations bound with a specific functional valency. After thorough kinetic analysis, we were able to distinguish two dissociation populations (faster and slower) by the curve fitting on the basis of a linear combination of dual exponential decay functions eq 1. Out of two off-rate constants ($k_{off,1}$, $k_{off,2}$) obtained, the slower rate constant accounted for the predominantly larger fraction (80−90%) of the decay curve and it was used to determine the on-rate constant (k_{on}) in the association phase eq 2. These two rate constants (k_{off}, k_{on}) are all reported in Table 2 along with their equilibrium dissociation constants (K_D).

Dissociation phase:

$$RU(t) = C_1 RU_{t=0}\, e^{-(k_{off,1})t} + C_2 RU_{t=0} e^{-(k_{off,2})t} \quad (1)$$

Association phase:

$$RU(t) = C_3(1 - e^{-(k_s)t}) + RU_{t=0} \quad (2)$$

Fitting parameters noted in each equation are defined as follows: $RU(t)$ = a response unit (ΔRU) at a specific time (t); $RU_{t=0}$ = RU at t = 0 (in either a dissociation or association phase); C_1, and C_2 = a coefficient that determines the weight of each dissociation component; $C_3 = k_{on}[conjugate]RU_A/(k_{on}[conjugate] + k_{off})$; $k_s = (k_{on}[conjugate] + k_{off})$. An equilibrium dissociation constant K_D (= k_{off}/k_{on}) reported for each G5-$(V)_n$ refers to a mean value obtained from multiple independent measurements ($n \geq 5$) per conjugate.

Confocal Microscopy. *Staphylococcus aureus* bacteria (ATCC 4012) were purchased from ATCC. The cells were stored in a frozen (−80 °C) suspension of 10% glycerol in nutrient broth with fetal bovine serum (FBS) until use. Prior to the study, a small amount of partially thawed bacterial suspension was spread on

a nutrient agar plate (Thermo Fisher Scientific IP-265) and incubated at 37 °C. The plated bacteria were harvested from the solid media after 48 h incubation and washed in sterile PBS (centrifugation at 9000 rpm for 10 min). For confocal microscopy, the bacterial cells were suspended in PBS (10^6 CFU/mL) and treated with 86 μM of either the conjugate **VIII** DTPA-G5-$(V)_{6.1}$-$(Fl)_{3.9}$ or **IX** Ac-G5-$(V)_{6.3}$-$(FITC)_{1.8}$, or the nontargeted control dendrimer, GA-G5-(FITC) for 30 min at room temperature. The treated cells were then washed with PBS and fixed in 4% paraformaldehyde in PBS for 10 min at room temperature. Cells were rinsed multiple times with PBS and then stained with Syto 59, a cell-permeable fluorescent DNA binding molecule (λ_{em} = 645 nm; red). Cells were washed with PBS and resuspended in PBS. Each bacterial cell suspension was applied onto a chambered cover glass and allowed for air-dry before mounting the slide in Prolong Gold Antifade (Life Technologies, Carlsbad, CA). Images were acquired using a Zeiss LSM 510-META laser scanning confocal microscope (Carl Zeiss Microscopy, LLC, Thornwood, NY) equipped with argon and helium−neon lasers. Fluorescence was measured using 488 nm (green) and 543 (red) excitation lines, and imaged at a 63-fold magnification.

Turbidity Assay. The assay was performed as previously described with minor modifications.[79] A stock solution of vancomycin or an equimolar concentration of a vancomycin conjugate was prepared in a brain-heart infusion (BHI) medium and 2-fold serial dilutions were made for each test compound on a 96-well flat bottom plate (100 μL per well). One hundred microliter of an inoculum of *Staphylococcus aureus* bacteria was added to each well at the concentration of 5×10^6 CFU/mL. After incubation of the plates at 37 °C for 24 h, bacterial growth was examined by optical microscopy and reading an optical density (O.D.) value at 650 nm by an ELISA plate reader.

Bacterial Isolation by IONPs. On the day of the experiment for bacterial isolation, each IONP suspension was agitated and an aliquot needed for the experiment was taken out. It was centrifuged at 9000 rpm for 10 min and washed with sterile PBS. The IONPs were resuspended in the PBS solution to a final concentration (2.5 mg/mL). A suspension of *Staphylococcus aureus* (ATCC 4012) bacteria in PBS ($\sim 1 \times 10^8$ CFU/mL) was split into several 1 mL aliquots in culture test tubes. Each test IONP (100 uL), prepared at the concentration of 2.5 mg/mL, was added to an aliquot of bacteria and the culture tube was incubated at room temperature for 15 min with occasional agitation. Subsequently, each tube was placed close to a magnet and left for 30 s. Then the supernatant was gently removed from each culture tube and saved. An amount of 1 mL of the sterile PBS solution was replenished to the tube and the IONPs were gently washed. After washing twice, the test tube was removed from the magnet and the IONPs were resuspended in PBS. A series of 10-fold dilutions were made for each supernatant and separately for each IONP isolated. The diluted sample (50 μL each) was placed on the agar plate, and the plate was incubated for 48 h at 37 °C. Distinguishable colonies were counted from each plate, and the mean number of bacterial colonies was estimated from the plot against dilution factors. Efficiency for isolating bacterial cells by each IONP was compared to the control level obtained by the same experiment performed with bacteria untreated.

***in Vitro* Cytotoxicity Assay.** Cytotoxicity of select vancomycin-conjugated PAMAM dendrimers to mammalian cells was evaluated in two cell lines including KB cells, a subline of the cervical carcinoma HeLa cells, and mouse melanoma B16−F10 cells, as described elsewhere.[71] After incubation of the cells for 3 days in the microtiter plate, each conjugate was added in a concentration-dependent manner. The number of cells grown was quantified by a colorimetric XTT assay[80] (sodium 3-[1-(phenylaminocarbonyl)-3,4-tetrazolium]-bis(4-methoxy-6-nitro)benzene sulfonic acid hydrate; Roche Mol. Biochem.) by reading absorbance at 492 nm relative to the reference value at 690 nm using on an ELISA reader (Synergy HT, BioTek).

Conflict of Interest: The authors declare no competing financial interest.

Acknowledgment. This work was supported by Michigan Nanotechnology Institute for Medicine and Biological Sciences (MNIMBS). S.K.C. thanks Undergraduate Research Opportunity Program (UROP) at University of Michigan for the UROP fellowship (JS).

Supporting Information Available: Experimental details, copies of characterization data (GPC and HPLC traces, UV−vis spectra, ^{1}H NMR spectra, MALDI-TOF mass spectra), and additional figures from SPR spectroscopy, the turbidity assay, and the cell cytotoxicity study. This material is available free of charge *via* the Internet at http://pubs.acs.org.

REFERENCES AND NOTES

1. Bihl, F.; Castelli, D.; Marincola, F.; Dodd, R. Brander, C. Transfusion-Transmitted Infections. *J. Transl. Med.* **2007**, *5*, 25.
2. Depcik-Smith, N. D.; Hay, S. N.; Brecher, M. E. Bacterial Contamination of Blood Products: Factors, Options, And Insights. *J. Clin. Apheresis* **2001**, *16*, 192–201.
3. Jacoby, G. A.; Archer, G. L. New Mechanisms of Bacterial Resistance to Antimicrobial Agents. *N. Engl. J. Med.* **1991**, *324*, 601–612.
4. Dajani, A. S.; Taubert, K. A.; Wilson, W.; Bolger, A. F.; Bayer, A.; Ferrieri, P.; Gewitz, M. H.; Shulman, S. T.; Nouri, S.; Newburger, J. W.; *et al.* Prevention of Bacterial Endocarditis: Recommendations by The American Heart Association. *Circulation* **1997**, *96*, 358–366.
5. Tipple, M. A.; Bland, L. A.; Murphy, J. J.; Arduino, M. J.; Panlilio, A. L.; Farmer, J. J.; Tourault, M. A.; Macpherson, C. R.; Menitove, J. E.; Grindon, A. J.; *et al.* Sepsis Associated with Transfusion of Red Cells Contaminated with Yersinia Enterocolitica. *Transfusion (Malden, MA, U.S.)* **1990**, *30*, 207–213.
6. Muder, R. R.; Yee, Y. C.; Rihs, J. D.; Bunker, M. *Staphylococcus Epidermidis* Bacteremia from Transfusion of Contaminated Platelets: Application of Bacterial DNA Analysis. *Transfusion (Malden, MA, U.S.)* **1992**, *32*, 771–774.
7. Cosgrove, S. E.; Sakoulas, G.; Perencevich, E. N.; Schwaber, M. J.; Karchmer, A. W.; Carmeli, Y. Comparison of Mortality Associated with Methicillin-Resistant and Methicillin-Susceptible *Staphylococcus Aureus* Bacteremia: A Meta-analysis. *Clin. Infect. Dis.* **2003**, *36*, 53–59.
8. Schmidt, M.; Sireis, W.; Seifried, E. Implementation of Bacterial Detection Methods into Blood Donor Screening—Overview of Different Technologies. *Transfusion Med. Hemother.* **2011**, *38*, 259–265.
9. Kell, A. J.; Stewart, G.; Ryan, S.; Peytavi, R.; Boissinot, M.; Huletsky, A.; Bergeron, M. G.; Simard, B. Vancomycin-Modified Nanoparticles for Efficient Targeting and Preconcentration of Gram-Positive and Gram-Negative Bacteria. *ACS Nano* **2008**, *2*, 1777–1788.
10. Kukowska-Latallo, J. F.; Candido, K. A.; Cao, Z.; Nigavekar, S. S.; Majoros, I. J.; Thomas, T. P.; Balogh, L. P.; Khan, M. K.; Baker, J. R., Jr Nanoparticle Targeting of Anticancer Drug Improves Therapeutic Response in Animal Model of Human Epithelial Cancer. *Cancer Res.* **2005**, *65*, 5317–5324.
11. Low, P. S.; Henne, W. A.; Doorneweerd, D. D. Discovery and Development of Folic-Acid-Based Receptor Targeting for Imaging and Therapy of Cancer and Inflammatory Diseases. *Acc. Chem. Res.* **2008**, *41*, 120–129.
12. Myc, A.; Majoros, I. J.; Thomas, T. P.; Baker, J. R., Jr. Dendrimer-Based Targeted Delivery of an Apoptotic Sensor in Cancer Cells. *Biomacromolecules* **2007**, *8*, 13–18.
13. Thomas, T. P.; Goonewardena, S. N.; Majoros, I. J.; Kotlyar, A.; Cao, Z.; Leroueil, P. R.; Baker, J. R. Folate-Targeted Nanoparticles Show Efficacy in the Treatment of Inflammatory Arthritis. *Arthritis Rheum.* **2011**, *63*, 2671–2680.
14. Majoros, I. J.; Williams, C. R.; Becker, A.; Baker, J. R., Jr Methotrexate Delivery *via* Folate Targeted Dendrimer-Based Nanotherapeutic Platform. *WIREs: Nanomed. Nanobiotechnol.* **2009**, *1*, 502–510.
15. Choi, S. K.; Thomas, T.; Li, M.; Kotlyar, A.; Desai, A.; Baker, J. R., Jr Light-Controlled Release of Caged Doxorubicin from Folate Receptor-Targeting PAMAM Dendrimer Nanoconjugate. *Chem. Commun. (Cambridge, U.K.)* **2010**, *46*, 2632–2634.

16. Walsh, C. Molecular Mechanisms that Confer Antibacterial Drug Resistance. *Nature (London, U.K.)* **2000**, *406*, 775–781.
17. Tipper, D. J. Mode of Action of β-Lactam Antibiotics. *Pharmacol. Ther.* **1985**, *27*, 1–35.
18. Velkov, T.; Thompson, P. E.; Nation, R. L.; Li, J. Structure−Activity Relationships of Polymyxin Antibiotics. *J. Med. Chem.* **2009**, *53*, 1898–1916.
19. Chung, H. J.; Reiner, T.; Budin, G.; Min, C.; Liong, M.; Issadore, D.; Lee, H.; Weissleder, R. Ubiquitous Detection of Gram-Positive Bacteria with Bioorthogonal Magnetofluorescent Nanoparticles. *ACS Nano* **2011**, *5*, 8834–8841.
20. Krishnamurthy, V. M.; Quinton, L. J.; Estroff, L. A.; Metallo, S. J.; Isaacs, J. M.; Mizgerd, J. P.; Whitesides, G. M. Promotion of Opsonization by Antibodies and Phagocytosis of Gram-Positive Bacteria by a Bifunctional Polyacrylamide. *Biomaterials* **2006**, *27*, 3663–3674.
21. Metallo, S. J.; Kane, R. S.; Holmlin, R. E.; Whitesides, G. M. Using Bifunctional Polymers Presenting Vancomycin and Fluorescein Groups To Direct Anti-Fluorescein Antibodies to Self-Assembled Monolayers Presenting D-Alanine-D-Alanine Groups. *J. Am. Chem. Soc.* **2003**, *125*, 4534–4540.
22. Rao, J.; Lahiri, J.; Isaacs, L.; Weis, R. M.; Whitesides, G. M. A Trivalent System from Vancomycin·D-Ala-D-Ala with Higher Affinity Than Avidin·Biotin. *Science (WAshington, DC, U.S.)* **1998**, *280*, 708–711.
23. Rao, J.; Whitesides, G. M. Tight Binding of a Dimeric Derivative of Vancomycin with Dimeric L-Lys-D-Ala-D-Ala. *J. Am. Chem. Soc.* **1997**, *119*, 10286–10290.
24. Rao, J.; Yan, L.; Lahiri, J.; Whitesides, G. M.; Weis, R. M.; Warren, H. S. Binding of a Dimeric Derivative of Vancomycin to L-Lys-D-Ala-D-Lactate in Solution and at a Surface. *Chem. Biol. (Cambridge, MA, U.S.)* **1999**, *6*, 353–359.
25. Rao, J.; Yan, L.; Xu, B.; Whitesides, G. M. Using Surface Plasmon Resonance to Study the Binding of Vancomycin and Its Dimer to Self-Assembled Monolayers Presenting D-Ala-D-Ala. *J. Am. Chem. Soc.* **1999**, *121*, 2629–2630.
26. Xing, B.; Yu, C.-W.; Ho, P.-L.; Chow, K.-H.; Cheung, T.; Gu, H.; Cai, Z.; Xu, B. Multivalent Antibiotics *via* Metal Complexes: Potent Divalent Vancomycins against Vancomycin-Resistant *Enterococci*. *J. Med. Chem.* **2003**, *46*, 4904–4909.
27. Gu, H.; Ho, P. L.; Tong, E.; Wang, L.; Xu, B. Presenting Vancomycin on Nanoparticles to Enhance Antimicrobial Activities. *Nano Lett.* **2003**, *3*, 1261–1263.
28. Gu, H.; Ho, P.-L.; Tsang, K. W. T.; Wang, L.; Xu, B. Using Biofunctional Magnetic Nanoparticles to Capture Vancomycin-Resistant *Enterococci* and Other Gram-Positive Bacteria at Ultralow Concentration. *J. Am. Chem. Soc.* **2003**, *125*, 15702–15703.
29. Walsh, C. T.; Fisher, S. L.; Park, I. S.; Prahalad, M.; Wu, Z. Bacterial Resistance to Vancomycin: Five Genes and One Missing Hydrogen Bond Tell the Story. *Chem. Biol. (Cambridge, MA, U.S.)* **1996**, *3*, 21–28.
30. Griffin, J. H.; Linsell, M. S.; Nodwell, M. B.; Chen, Q. Q.; Pace, J. L.; Quast, K. L.; Krause, K. M.; Farrington, L.; Wu, T. X.; Higgins, D. L.; *et al*. Multivalent Drug Design. Synthesis and *in Vitro* Analysis of an Array of Vancomycin Dimers. *J. Am. Chem. Soc.* **2003**, *125*, 6517–6531.
31. Hong, S.; Leroueil, P. R.; Majoros, I. J.; Orr, B. G.; Baker, J. R., Jr; Banaszak Holl, M. M. The Binding Avidity of a Nanoparticle-Based Multivalent Targeted Drug Delivery Platform. *Chem. Biol. (Cambridge, MA, U.S.)* **2007**, *14*, 107–115.
32. Mammen, M.; Choi, S. K.; Whitesides, G. M. Polyvalent Interactions in Biological Systems: Implications for Design and Use of Multivalent Ligands and Inhibitors. *Angew. Chem., Int. Ed.* **1998**, *37*, 2754–2794.
33. Roy, R. Syntheses and Some Applications of Chemically Defined Multivalent Glycoconjugates. *Curr. Opin. Struct. Biol.* **1996**, *6*, 692–702.
34. Lee, Y. C.; Lee, R. T. Carbohydrate-Protein Interactions: Basis of Glycobiology. *Acc. Chem. Res.* **1995**, *28*, 321–327.
35. Kiessling, L. L.; Gestwicki, J. E.; Strong, L. E. Synthetic Multivalent Ligands in the Exploration of Cell-Surface Interactions. *Curr. Opin. Chem. Biol.* **2000**, *4*, 696–703.
36. Tomalia, D. A.; Baker, H.; Dewald, J.; Hall, M.; Kallos, G.; Martin, S.; Roeck, J.; Ryder, J.; Smith, P. A New Class of Polymers: Starburst-Dendritic Macromolecules. *Polymer J.* **1985**, *17*, 117–132.
37. Tomalia, D. A.; Naylor, A. M.; Goddard, William A. I. Starburst Dendrimers: Molecular-Level Control of Size, Shape, Surface Chemistry, Topology, and Flexibility from Atoms to Macroscopic Matter. *Angew. Chem., Int. Ed. Engl.* **1990**, *29*, 138–175.
38. Majoros, I.; Baker, J., Jr. *Dendrimer-Based Nanomedicine*; Pan Stanford: Hackensack, NJ, 2008; p 436.
39. Thomas, T. P.; Choi, S. K.; Li, M.-H.; Kotlyar, A.; Baker, J. R., Jr Design of Riboflavin-Presenting PAMAM Dendrimers as a New Nanoplatform for Cancer-Targeted Delivery. *Bioorg. Med. Chem. Lett.* **2010**, *20*, 5191–5194.
40. Thomas, T. P.; Shukla, R.; Kotlyar, A.; Liang, B.; Ye, J. Y.; Norris, T. B.; Baker, J. R., Jr. Dendrimer-Epidermal Growth Factor Conjugate Displays Superagonist Activity. *Biomacromolecules* **2008**, *9*, 603–609.
41. Svenson, S.; Tomalia, D. A. Dendrimers in Biomedical Applications-Reflections on the Field. *Adv. Drug Delivery Rev.* **2005**, *57*, 2106–2129.
42. Baker, J. R., Jr. Dendrimer-Based Nanoparticles for Cancer Therapy. *Hematol. Am. Soc. Hematol. Educ. Program* **2009**, *2009*, 708–719.
43. Liang, C.; Fréchet, J. M. J. Applying Key Concepts From Nature: Transition State Stabilization, Pre-concentration and Cooperativity Effects in Dendritic Biomimetics. *Prog. Polym. Sci.* **2005**, *30*, 385–402.
44. Mullen, D.; Borgmeier, E.; Desai, A.; van Dongen, M.; Barash, M.; Cheng, X. m.; Baker, J. R., Jr.; Banaszak Holl, M. Isolation and Characterization of Dendrimer with Precise Numbers of Functional Groups. *Chem.—Eur. J.* **2010**, *16*, 10675–10678.
45. Mullen, D. G.; Fang, M.; Desai, A.; Baker, J. R., Jr; Orr, B. G.; Banaszak Holl, M. M. A Quantitative Assessment of Nanoparticle-Ligand Distributions: Implications for Targeted Drug and Imaging Delivery in Dendrimer Conjugates. *ACS Nano* **2010**, *4*, 657–670.
46. Cloninger, M. J. Biological Applications of Dendrimers. *Curr. Opin. Chem. Biol.* **2002**, *6*, 742–748.
47. Esfand, R.; Tomalia, D. A. Poly(amidoamine) (PAMAM) Dendrimers: From Biomimicry to Drug Delivery and Biomedical Applications. *Drug Discovery Today* **2001**, *6*, 427–436.
48. Medina, S. H.; El-Sayed, M. E. H. Dendrimers as Carriers for Delivery of Chemotherapeutic Agents. *Chem. Rev. (Washington, DC, U.S.)* **2009**, *109*, 3141–3157.
49. Long, D.; Aggen, J. B.; Chinn, J.; Choi, S.-K.; Christensen, B. G.; Fatheree, P. R.; Green, D.; Hegde, S.; Judice, K.; Kaniga, K.; *et al*. Exploring the Positional Attachment of Glycopeptide/β-Lactam Heterodimers. *J. Antibiot.* **2008**, *61*, 603–614.
50. Caravan, P.; Ellison, J. J.; McMurry, T. J.; Lauffer, R. B. Gadolinium(III) Chelates as MRI Contrast Agents: Structure, Dynamics, and Applications. *Chem. Rev. (Washington, DC, U.S.)* **1999**, *99*, 2293–2352.
51. Nolan, E. M.; Ryu, J. W.; Jaworski, J.; Feazell, R. P.; Sheng, M.; Lippard, S. J. Zinspy Sensors with Enhanced Dynamic Range for Imaging Neuronal Cell Zinc Uptake and Mobilization. *J. Am. Chem. Soc.* **2006**, *128*, 15517–15528.
52. Mullen, D. G.; Desai, A. M.; Waddell, J. N.; Cheng, X.-m.; Kelly, C. V.; McNerny, D. Q.; Majoros, I. n. J.; Baker, J. R., Jr.; Sander, L. M.; Orr, B. G.; *et al*. The Implications of Stochastic Synthesis for the Conjugation of Functional Groups to Nanoparticles. *Bioconjugate Chem.* **2008**, *19*, 1748–1752.
53. Choi, S. K.; Leroueil, P.; Li, M.-H.; Desai, A.; Zong, H.; Van Der Spek, A. F. L.; Baker, J. R., Jr. Specificity and Negative Cooperativity in Dendrimer−Oxime Drug Complexation. *Macromolecules* **2011**, *44*, 4026–4029.
54. Gu, F.; Zhang, L.; Teply, B. A.; Mann, N.; Wang, A.; Radovic-Moreno, A. F.; Langer, R.; Farokhzad, O. C. Precise Engineering of Targeted Nanoparticles by Using Self-Assembled Biointegrated Block Copolymers. *Proc. Natl. Acad. Sci. U.S.A.* **2008**, *105*, 2586–2591.

55. Zhu, Y.; Qian, H.; Drake, Bethany A.; Jin, R. Atomically Precise $Au_{25}SR_{18}$ Nanoparticles as Catalysts for the Selective Hydrogenation of alpha,beta-Unsaturated Ketones and Aldehydes. *Angew. Chem. Intl. Ed.* **2010**, *49*, 1295–1298.
56. Qian, H.; Jin, R. Controlling Nanoparticles with Atomic Precision: The Case of $Au_{144}(SCH_2CH_2Ph)_{60}$. *Nano Lett.* **2009**, *9*, 4083–4087.
57. Li, M.-H.; Choi, S. K.; Thomas, T. P.; Desai, A.; Lee, K.-H.; Kotlyar, A.; Banaszak Holl, M. M.; Baker, J. R., Jr. Dendrimer-Based Multivalent Methotrexates as Dual Acting Nanoconjugates for Cancer Cell Targeting. *Eur. J. Med. Chem.* **2012**, *47*, 560–572.
58. Plantinga, A.; Witte, A.; Li, M.-H.; Harmon, A.; Choi, S. K.; Banaszak Holl, M. M.; Orr, B. G.; Baker, J. R., Jr.; Sinniah, K. Bioanalytical Screening of Riboflavin Antagonists for Targeted Drug Delivery—A Thermodynamic and Kinetic Study. *ACS Med. Chem. Lett* **2011**, *2*, 363–367.
59. Cooper, M. A.; Fiorini, M. T.; Abell, C.; Williams, D. H. Binding of Vancomycin Group Antibiotics to D-Alanine and D-Lactate Presenting Self-Assembled Monolayers. *Bioorg. Med. Chem.* **2000**, *8*, 2609–2616.
60. Ober, R. J.; Caves, J.; Sally Ward, E. Analysis of Exponential Data Using a Noniterative Technique: Application to Surface Plasmon Experiments. *Anal. Biochem.* **2003**, *312*, 57–65.
61. Arranz-Plaza, E.; Tracy, A. S.; Siriwardena, A.; Pierce, J. M.; Boons, G. J. High-Avidity, Low-Affinity Multivalent Interactions and the Block to Polyspermy in Xenopus Laevis. *J. Am. Chem. Soc.* **2002**, *124*, 13035–13046.
62. Adler, P.; Wood, S. J.; Lee, Y. C.; Lee, R. T.; Petri, W. A., Jr; Schnaar, R. L. High Affinity Binding of the Entamoeba Histolytica Lectin to Polyvalent *N*-Acetylgalactosaminides. *J. Biol. Chem.* **1995**, *270*, 5164–5171.
63. Page, M. I.; Jencks, W. P. Entropic Contributions to Rate Accelerations in Enzymic and Intramolecular Reactions and the Chelate Effect. *Proc. Natl. Acad. Sci. U.S.A.* **1971**, *68*, 1678–1683.
64. Mackay, J. P.; Gerhard, U.; Beauregard, D. A.; Williams, D. H.; Westwell, M. S.; Searle, M. S. Glycopeptide Antibiotic Activity and the Possible Role of Dimerization: A Model for Biological Signaling. *J. Am. Chem. Soc.* **1994**, *116*, 4581–4590.
65. Hunter, C. A.; Anderson, H. L. What is Cooperativity? *Angew. Chem. Intl. Ed.* **2009**, *48*, 7488–7499.
66. Krishnamurthy, V. M.; Semetey, V.; Bracher, P. J.; Shen, N.; Whitesides, G. M. Dependence of Effective Molarity on Linker Length for an Intramolecular Protein-Ligand System. *J. Am. Chem. Soc.* **2007**, *129*, 1312–1320.
67. Chung, H. S.; Yao, Z.; Goehring, N. W.; Kishony, R.; Beckwith, J.; Kahne, D. Rapid β-Lactam-Induced Lysis Requires Successful Assembly of the Cell Division Machinery. *Proc. Natl. Acad. Sci. U.S.A.* **2009**, *106*, 21872–21877.
68. Lunde, C. S.; Hartouni, S. R.; Janc, J. W.; Mammen, M.; Humphrey, P. P.; Benton, B. M. Telavancin Disrupts the Functional Integrity of the Bacterial Membrane through Targeted Interaction with the Cell Wall Precursor Lipid II. *Antimicrob. Agents Chemother.* **2009**, *53*, 3375–3383.
69. Calabretta, M. K.; Kumar, A.; McDermott, A. M.; Cai, C. Antibacterial Activities of Poly(amidoamine) Dendrimers Terminated with Amino and Poly(ethylene glycol) Groups. *Biomacromolecules* **2007**, *8*, 1807–1811.
70. Leroueil, P. R.; Hong, S.; Mecke, A.; Baker, J. R.; Orr, B. G.; Banaszak Holl, M. M. Nanoparticle Interaction with Biological Membranes: Does Nanotechnology Present a Janus Face? *Acc. Chem. Res.* **2007**, *40*, 335–342.
71. Thomas, T. P.; Majoros, I.; Kotlyar, A.; Mullen, D.; Banaszak Holl, M. M.; Baker, J. R. Cationic Poly(amidoamine) Dendrimer Induces Lysosomal Apoptotic Pathway at Therapeutically Relevant Concentrations. *Biomacromolecules* **2009**, *10*, 3207–3214.
72. Lauffer, R. B. Paramagnetic Metal Complexes as Water Proton Relaxation Agents for NMR Imaging: Theory and Design. *Chem. Rev. (Washington, DC, U.S.)* **1987**, *87*, 901–927.
73. Byegård, J.; Skarnemark, G.; Skålberg, M. The Stability of Some Metal EDTA, DTPA and DOTA Complexes: Application as Tracers in Groundwater Studies. *J. Radioanal. Nucl. Chem.* **1999**, *241*, 281–290.
74. Laurent, S.; Forge, D.; Port, M.; Roch, A.; Robic, C.; Vander Elst, L.; Muller, R. N. Magnetic Iron Oxide Nanoparticles: Synthesis, Stabilization, Vectorization, Physicochemical Characterizations, and Biological Applications. *Chem. Rev. (Washington, DC, U.S.)* **2008**, *108*, 2064–2110.
75. Li, B.; Logan, B. E. Bacterial Adhesion to Glass and Metal-Oxide Surfaces. *Colloids Surf., B* **2004**, *36*, 81–90.
76. Brown, G. E.; Henrich, V. E.; Casey, W. H.; Clark, D. L.; Eggleston, C.; Felmy, A.; Goodman, D. W.; Grätzel, M.; Maciel, G.; McCarthy, M. I.; *et al*. Metal Oxide Surfaces and Their Interactions with Aqueous Solutions and Microbial Organisms. *Chem. Rev. (Washington, DC, U.S.)* **1998**, *99*, 77–174.
77. Majoros, I. J.; Thomas, T. P.; Mehta, C. B.; Baker, J. R., Jr. Poly(amidoamine) Dendrimer-Based Multifunctional Engineered Nanodevice for Cancer Therapy. *J. Med. Chem.* **2005**, *48*, 5892–5899.
78. MacKenzie, C. R.; Hirama, T.; Deng, S.-j.; Bundle, D. R.; Narang, S. A.; Young, N. M. Analysis by Surface Plasmon Resonance of the Influence of Valence on the Ligand Binding Affinity and Kinetics of an Anti-carbohydrate Antibody. *J. Biol. Chem.* **1996**, *271*, 1527–1533.
79. Myc, A.; Horn, R.; Hamouda, T.; Baker, J. R., Fungicidal Effect of a "Hybrid" Surfactant Lipid Preparation (SLP) on Candida Ssp. In 99th General Meeting of American Society for Microbiology, Chicago, IL, **1999**.
80. Roehm, N. W.; Rodgers, G. H.; Hatfield, S. M.; Glasebrook, A. L. An Improved Colorimetric Assay for Cell Proliferation and Viability Utilizing the Tetrazolium Salt XTT. *J. Immunol. Methods* **1991**, *142*, 257–265.